J. Phys.: Condens. Matter **21** (2009) 183001 (19pp) doi:10.1088/0953-8984/21/18/183001

TOPICAL REVIEW

Silicon oxidation by ozone

Christian K Fink[1], **Ken Nakamura**[2], **Shingo Ichimura**[2] **and Stephen J Jenkins**[1]

[1] Department of Chemistry, University of Cambridge, Cambridge CB2 1EW, UK
[2] National Institute of Advanced Industrial Science and Technology (AIST), Tsukuba Central 2, 1-1-1 Umezono, Tsukuba, Ibaraki 305-8568, Japan

E-mail: sjj24@cam.ac.uk

Received 31 January 2009
Published 11 March 2009
Online at stacks.iop.org/JPhysCM/21/183001

Abstract
Understanding the oxidation of silicon has been an ongoing challenge for many decades. Ozone has recently received considerable attention as an alternative oxidant in the low temperature, damage-free oxidation of silicon. The ozone-grown oxide was also found to exhibit improved interface and electrical characteristics over a conventionally dioxygen-grown oxide. In this review article, we summarize the key findings about this alternative oxidation process. We discuss the different methods of O_3 generation, and the advantages of the ozone-grown Si/SiO_2 interface. An understanding of the growth characteristics is of utmost importance for obtaining control over this alternative oxidation process.

(Some figures in this article are in colour only in the electronic version)

Contents

1. Introduction

The continued dominance of silicon as the semiconducting material of first choice within the microelectronics industry is, arguably, due primarily to the ease with which insulating silica may be grown upon it. Aside from any desirable intrinsic electronic properties of silicon, the ability to fabricate devices on wafers at the nanoscale depends upon this essential interfacial property. The continuing drive towards miniaturization, however, places ever greater demands upon the resulting oxide, particularly in the sub-4 nm thickness regime, where it exhibits a compositional and structural transition region extending up to a nanometre in depth [1]. The insulating properties of SiO_2 can therefore be compromised, leading to device failure.

Conventional oxide growth involves exposure of silicon to molecular dioxygen at high temperatures (usually greater than 800 °C [2, 3]) in order to achieve a fast oxide growth rate and ensure the high quality Si/SiO_2 interface needed for device applications. As an alternative strategy, low temperature oxidation would not only reduce the risk of inducing dopant migration, but also enable the processing of temperature-sensitive materials. Among various approaches, advanced low temperature oxidation methods include microwave plasma

oxidation, photo-oxidation in O_2, and different techniques using ozone (O_3) as oxidant. It is this latter approach that forms the basis of this review.

Ozone is more environmentally friendly than other oxidizing species such as N_2O and NO_2, since simply by heating it decomposes into molecular oxygen [4]. Compared to other radical oxygen species, O_3 can be generated in high concentrations, while the molecules exhibit only low kinetic energies according to the thermal velocity distribution. This is a clear advantage over plasma oxidation techniques, which often cause sample damage due to highly energetic particle bombardment. Similarly, photo-oxidation in O_2 requires irradiation by high energy photons (>7.2 eV), which increases the risk of defect formation at the interface [5].

While ozone is well known for its beneficial role in the upper atmosphere (due to its photochemistry ozone acts as a shield for harmful ultraviolet light), it is usually less well known that it is used in large volumes in large-scale industries such as water purification and paper and pulp processing [6]. In the semiconductor industry, the chemical reactivity of ozone has already found applications in the cleaning of wafers.

In 1989, the first to study ozone for silicon oxidation was Chao *et al* [7]. The authors observed an increase in the oxidation rate when O_3 was present at low concentration in O_2 gas. The potential of ozone for low temperature oxidation was soon recognized by Kazor *et al* [8, 9], and with the development of high-purity ozone generators [10, 11, 4] silicon oxidation by ozone has turned into a vibrant research field. In particular, a series of experiments has revealed that the Si/SiO_2 interface formed by the more reactive O_3 is of higher quality than the interface formed by regular O_2. Amongst these advantages, the ozone-grown interface exhibits less strain [12] and the notorious transition layer is reduced [13–15]. Ozone's oxide has also been tested for MOS-FET operations, where improved reliability characteristics were observed due to the improved interface properties [16].

Most recently, it was shown that the oxidation rate of UV-light excited ozone did not depend on the orientation of the Si crystal surface, which enabled the growth of a high quality oxide film at room temperature even on polycrystalline silicon [17].

Because of these advantages in the oxidation of silicon, ozone has also been tested in the oxidation of other materials, most prominently metal oxides. These materials exhibit a high dielectric constant (κ) and are therefore heavily investigated to replace the silicon oxide, which exhibits only a low dielectric constant, to allow further miniaturization of semiconductor devices.

This topical review will summarize and connect the available literature in the field of silicon oxidation by ozone. First, the different types of ozone generators will be introduced and discussed. Then, the advantages of ozone as oxidant will be presented in more detail. This is followed by an investigation of the growth characteristics. Here, we will find that the growth process is influenced by many parameters, which make a direct comparison between the growth studies difficult. Therefore, due to missing pieces in the puzzle, we will provide a qualitative picture of the oxidation by ozone. Finally, a brief overview of other oxide materials will be given, where ozone has been successfully applied as an oxidant.

2. Ozone generators

Here, we present a brief overview of the type of ozone generators employed in the study of silicon oxidation by ozone. Chao *et al* [7], who originally studied the potential of ozone as a more reactive oxidant in the oxidation of silicon, employed a commercially available ozone generator, which uses a low pressure mercury UV-light source 'UV/O_2' (two main wavelengths at 185 and 254 nm, at a ratio ≈1:10). This setup, however, only generated an O_3 concentration of 2.25 ppm in the O_2 stream. In order to avoid any UV exposure of the silicon sample, since high energy photons might lead to defect formation at the interface, the UV–ozone generator is kept outside the oxidizing furnace. The same type of ozone generator was also employed by Cui and co-workers [18], who achieved a concentration of 950 ppm of O_3 in the O_2 gas.

Kazor and Boyd [8, 9] used a barrier discharge ozonizer (BDO), sometimes also called silent discharge ozonizer [19], reaching higher O_3 concentrations between 3 and 4% in the O_2 gas. In this approach an AC voltage of several kV is applied across two dielectric coated electrodes, between which O_2 gas is pumped. The electric field produces an avalanche of electrons that directly dissociate the O_2 molecules into O atoms, which subsequently form O_3 molecules. Thus the oxidizing gas pumped into the oxidizing chamber is a mixture of O_2, O_3, and O (stated with decreasing concentration).

To move beyond the low-concentration limit, Ichimura and co-workers developed several types of high-concentration (>70%) O_3 generators [10, 20, 11, 21, 4] and tested their applicability in the oxidation of silicon. A key issue for these generator types is the safe handling of the highly-concentrated ozone gas, since at these high ozone concentrations the potential danger of an explosive conversion of O_3 into O_2 has to be considered.

Therefore, any factor, which would favour such an explosive conversion (e.g. catalytic exposure, sudden temperature changes, or mechanical vibrations) has to be eliminated in the generator design (figure 1).

It has also been confirmed that O_3, despite its high concentration, exhibits a long enough lifetime in the gas phase to react with the silicon sample, as long as the temperature (<100 °C) and the pressure ($<4 \times 10^4$ Pa) are controlled [21]. Thus, to avoid decomposition of gas-phase ozone, the heating should be limited to the surface only.

The first type of high-concentration O_3 generator ('Ozone Jet Generator I') [10, 20] utilizes the difference in equilibrium vapour pressure between the liquid phases of O_3 and O_2. These vapour pressures differ by three-to-four orders of magnitude at 90 K, which are the typical temperature conditions during the ozone 'collecting' cycle.

This allows to selectively liquefy ozone from the incoming O_3/O_2 mixture gas, which is generated from a commercial ozonizer with an ozone concentration of ≈5%. In this way, liquefied ozone is progressively stored in an ozone vessel with a volume of <0.5 cm^3 (in the most recent design, this volume

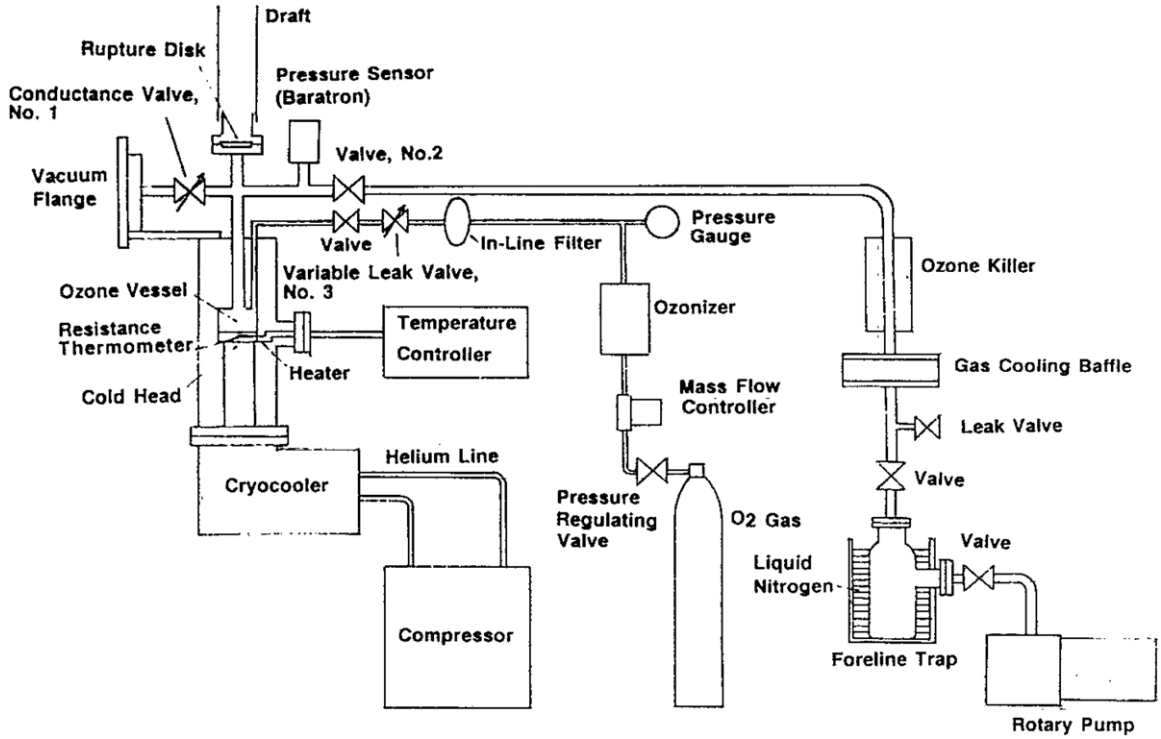

Figure 1. Ozone Jet Generator I: the first type of high-concentration ozone generator as used for low temperature oxidation of silicon. Reprinted with permission from [10]. ©1991, American Institute of Physics.

was further increased to store over 5 cm^3 of liquid ozone). Then, upon slowly heating this ozone vessel, the liquid ozone vaporizes and high-purity ozone gas passes through a nozzle into the oxidation chamber. Due to an undesired trapping of impurity gases, however, the ozone vessel has to be evacuated after only a few collection cycles.

To ensure *continuous* high-concentration O_3 supply, this generator type has been further developed to comprise four ozone vessels ('Ozone Jet Generator II') [4], which independently address the four modes of operation (i.e. accumulation/storage; vaporization/supply; evacuation; and cooling). Still, one major limitation is that this generator type (due to safe-handling considerations) can only supply high-concentration O_3 at low pressure conditions ($<2 \times 10^3$ Pa). This type was therefore mainly used to study how ozone adsorbs on the silicon surface and its initial oxidation stage.

In order to supply high-concentration ozone at high pressure conditions (between 10^3 and 10^5 Pa), and thus study the formation of thin oxide films, an entirely different generator was developed, which employs an adsorption–desorption technique via a silica gel ('ozone silica gel') [11]. Here, instead of liquefying the ozone, the O_3/O_2 gas from the commercial ozonizer passes through a column of silica gel, which is kept at ≈213 K. In this gel, the O_3 molecules selectively adsorb. In contrast to the liquid storage, O_3 is stabilized in this adsorption state, which prevents a spontaneous decomposition.

Subsequently, to supply the O_3 into the oxidation chamber, the silica gel is heated to room temperature and the adsorbed ozone gas desorbs. Even though this generator allows in principle a maximum ozone concentration of ≈70%, even at high pressure conditions (10^5 Pa), to strictly avoid any explosive decomposition the ozone concentration is usually kept below 30%. To continuously supply high-concentration ozone gas, this generator consists of three such ozone columns containing silica gel, which sequentially cycle through the three modes of operation (i.e. cooling; adsorption/storage; desorption/supply).

To achieve a controllable supply of ozone molecules, a collimated hyperthermal O_3 beam was generated by a technique based on pulsed laser deposition (PLD) [21]. In this design, high-purity O_3 gas, supplied from the previously-described ozone jet generator, passed over a sapphire plate, which was cooled to 30 K, and formed a 100 μm thick solid ozone film. A pulsed KrF excimer laser ($\lambda = 254$ nm) is aimed at this film and ablates for each laser shot a constant flux of O, O_2 and O_3 molecules (a total of $\approx 10^{17}$ molecules cm^{-2}/shot) with a small angular spread (6°). The O_3 concentration in the beam was estimated to be ≈80%, which decreased to <10% at higher laser fluences. Nevertheless, since the species received higher translational energy, and in addition the O atom concentration increased, higher laser fluences also resulted in a faster oxidation rate. In general, since the oxygen species in the beam have a much higher kinetic energy than thermal O_3, the oxidation rate by PLD was faster than by any other generator type. The kinetic energy (KE) distribution was found to be very similar for all three oxygen species, and revealed a mean KE of 0.4 eV and a maximum KE of 2 eV per molecule or atom.

Finally, a high-concentration ozone generator was used in combination with a laser source, which directly illuminated the O_3 gas in the oxidation chamber (UV/O_3) [22]. Different

Table 1. O_3 generators used in the oxidation of silicon by ozone.

Type	Abbrev.	O_3 conc (%)	References	Remarks
UV-based generator (Hg lamp)	UV/O_2	<0.1	[7, 18]	
Barrier discharge ozonizer	BDO	3–4	[19]	
Ozone jet generator	OJG	99	[10, 20, 4]	Low pressure ($<2 \times 10^3$ Pa)
Ozone silica gel	OSG	30–70	[11]	High pressure ($<10^5$ Pa)
Pulsed laser deposition	PLD		[21]	Hyperthermal beam
UV-assisted (KrF lamp)	UV/O_3		[22]	Additional UV source

irradiation conditions were tested, including UV-light in a perpendicular and horizontal direction with respect to the silicon sample. The direct UV irradiation of the sample was found not to be mandatory for the increased oxidation rate. Instead, the UV induces the dissociation of O_3, leading to a direct supply of atomic oxygens for the oxidation, which allows a fast oxidation rate even at room temperature. Since O_3 has a high adsorption coefficient in the UV range between 220 and 310 nm, a KrF excimer laser source ($\lambda = 248$ nm) has been used, which provides the necessary high photon density. In comparison, the photo-oxidation of O_2 [23, 24] is less effective, since O_2's photodissociation rate is only low and necessitates shorter laser wavelengths (usually 172 or 126 nm), which have a short penetration depth in air and are prone to induce defects at the Si/SiO_2 interface [25]. In contrast, the UV-light to dissociate O_3 does not cause any damage to the silicon sample.

A summary of the generator types is given in table 1 while further details on the oxidation kinetics and oxidation rates of each generator type will be discussed in a later section.

3. Advantages of oxidation by ozone

This section summarizes the experiments which have revealed three advantages of using ozone as oxidant. First, the more reactive O_3 gives a faster oxidation rate, which allows the silicon oxidation to proceed at much lower temperatures. Second, the oxidation rate in O_3 was found to be independent of silicon's crystallographic orientation. Finally, the ozone-grown oxide film yields a Si/SiO_2 interface of higher quality than a conventionally grown oxide film (800–900 °C). In this discussion we will include the processing conditions (temperature and ozone concentration), since they were found to influence the growth rate and film characteristics to a certain extent.

3.1. Fast oxidation at low temperatures

Originally, O_3 has been used as a more reactive oxidant to increase the oxidation rate and thus lower the oxidation temperature [7, 26]. By adding photogenerated O_3 (UV/O_2 with 2.25 ppm O_3) to the O_2 gas at oxidation temperatures of 700–800 °C the oxide film was for the same oxidation time 50–100% thicker than in pure O_2 [7]. At higher ozone concentrations (BDO, 3–4 O_3) and lower temperatures (400–800 °C) this growth enhancement was even more pronounced [9, 26] and was found to increase with lower oxidation temperatures (e.g. at 400 °C the O_3/O_2 gas formed an oxide film which was 400% thicker than in pure O_2 [9]). Thus, at a temperature of 550 °C oxidation in O_3 gave a comparable growth rate to oxidation in pure O_2 at 850 °C [9].

As an alternative, low temperature oxidation reduces the risk of inducing dopant migration and in addition enables processing of temperature-sensitive materials (e.g. plastic and glass substrates). Most recently, this growth rate enhancement was even further boosted, allowing oxidation at room temperature. By exposing high-concentration O_3 gas directly to UV-light (UV/O_3), high quality oxide films were even grown at room temperature [25, 17]. More details about the growth characteristic in an O_3-containing oxidant gas will be discussed in the specified section below.

3.2. Growth rate independent of surface orientation

Conventional oxidation by molecular oxygen shows a strong dependence on the surface orientation, leading to significantly faster growth rates on Si surfaces with {111} orientation than {001}. Therefore, on poly-silicon, which exhibits various crystallographic orientations separated by grain boundaries, oxidation in O_2 leads to the formation of non-uniform films. In contrast, oxygen atoms oxidize silicon at a rate independent of its orientation [1].

To confirm the same behaviour for the oxidant ozone, Kameda *et al* [17] studied the oxidation of various silicon orientations by UV-excited ozone at temperatures of 20 and 400 °C. The authors found that the oxide film formed on Si{111} and Si{001} after UV–ozone exposure had the same thickness independent of the surface orientation. Similarly, the oxidation of poly-silicon by UV–ozone resulted in a homogeneous oxide film (figure 2), which even at room temperature resulted in the formation of a high quality Si/SiO_2 interface with a low leakage current and a high breakdown voltage.

3.3. Improved interface characteristics

Two kinds of transition layers have been identified at the Si/SiO_2 interface, namely the compositional and the structural transition layers [1]. The compositional transition layer corresponds to the formation of a substoichiometric oxide, SiO_x, where the Si atoms are not fully oxidized (thus species of Si^{1+}, Si^{2+} and Si^{3+} are present). This suboxide lowers the insulating qualities and the lifetime of the oxide and is usually limited to one-to-two atomic layers within the oxide.

The structural transition layer, in contrast, is due to the volumetric expansion of the SiO_2 film relative to the silicon lattice, which implies a strained region, usually found on both sides of the interface (Si and SiO_2). On the Si side of the

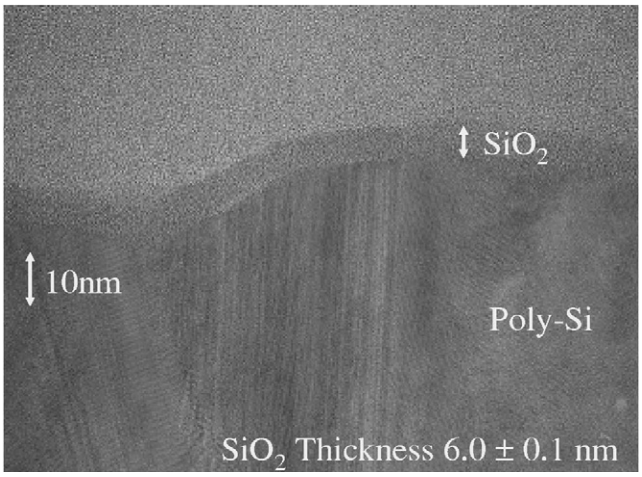

Figure 2. Transmission electron microscopy image of cross section of poly-Si with SiO_2 film. A homogeneous 6.0 nm thick SiO_2 film formed after UV–ozone exposure for 30 min at 20 °C (thickness of SiO_2 film and 10 nm reference labelled). Reprinted with permission from [17]. ©2007, The Electrochemical Society.

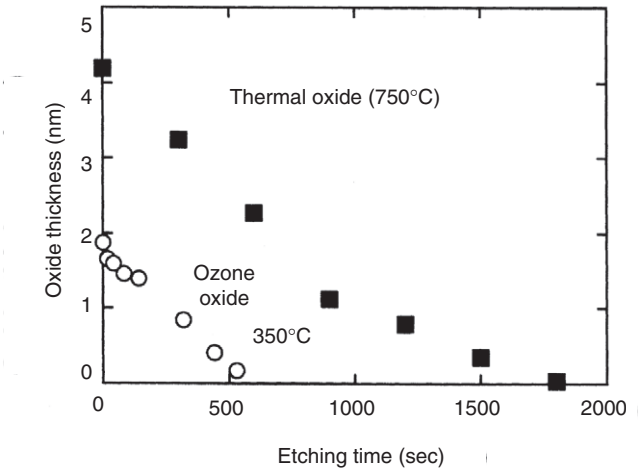

Figure 3. Oxide thickness on Si{001} during etching process (0.1 wt% HF solution at 25 °C) for thermally grown oxide (■, wet oxidation at 750 °C) and ozone-grown oxide (○, $p = 10^5$, $T = 350$ °C, $c > 30\%$). Reprinted with permission from [29]. ©2000, Elsevier.

interface, this distortion is limited to only one or two layers, while on the oxide side this region has been found for thermally grown oxide to extend up to 1 nm thickness. The structure of this transition region exhibits a distortion of the Si–O bond lengths and bond angles with respect to bulk SiO_2.

Experimentally, the existence of a transition layer is inferred from changes in the XPS spectrum, HF etching rate, MEIS, and FTIR vibrational analysis. These techniques have been applied to elucidate the interface properties of the ozone-grown oxide.

3.3.1. Diminished interfacial transition layer. The first indication that ozone gives improved interface characteristics over a conventionally grown oxide, was found by Awaji *et al* [13]. The authors applied difference x-ray reflectivity to study the silicon oxide growth in O_2 and O_3 (5%)/O_2 (generated by a discharge ozonizer, BDO-type) at temperatures between 800 and 1000 °C. They found an interfacial layer of ≈1 nm thickness which exhibited a higher density than bulk SiO_2. The thickness of this interfacial layer, however, decreased with higher oxidation temperatures and also in the presence of the more reactive ozone oxidant. Subsequently, the ozone-grown oxide and its interface properties were studied in greater detail.

3.3.2. Constant HF etching rate. The etching rate of silicon oxide in hydrofluoric acid (HF) is sensitive to the density, porosity, and composition of the oxide film and thus allows to probe the quality of the oxide. The HF etching rate of ozone-grown oxide has been studied and compared to thermally grown and native oxide[3] [14, 27, 28].

Whereas the thermally grown oxide showed two etching rates, depending on the film depth, the etching rate of the ozone-grown oxide was found to be independent of the film depth (see figure 3). For the O_2-grown film, the etching rate decreased at a thickness of around 1.2 nm, which indicates a transition region of higher density near the Si/SiO_2 interface. In contrast, high-concentration O_3 exposure at low pressure ($p = 10^{-4}$ Pa) [14] and high pressure ($p = 10^5$ Pa) [27] conditions confirmed that the etching rate of the ozone-grown oxide is constant even close to the interface.

The conditions of how the oxidant O_3 is supplied, however, were found to be critical for the quality of the ozone oxide. Since very long exposure times are necessary to form the oxide film at room temperature, the lifetime of the reactive O_3 starts to play a significant role. By filling the processing chamber with high-concentration O_3 gas and storing, instead of replacing, the gas during the oxidation process, O_3 decomposes into the less reactive O_2. It was found that in these processing conditions the HF etching rates of the films were as high as those of a native oxide [27]. In contrast, by constantly supplying the O_3 gas [28], a film of comparable quality to the best thermally grown oxide was formed even at room temperature.

Interestingly, it was also observed that it is possible to upgrade the poor film quality of a native oxide by exposure to ozone at appropriate temperature conditions [28]. The native oxide exhibits a high HF etching rate, which is nevertheless constant throughout the film. After ozone exposure above 350 °C, the etching rate of the oxide decreased, which relates to an increase in film density, and stayed independent of the film depth. In contrast, an already present structural transition layer of a thermally grown oxide was not affected by O_3 oxidation [28].

3.3.3. Less Si displaced at interface. To explain the observations of the different HF etching rates, the structural properties of the SiO_2 film near the Si/SiO_2 interface were studied by medium energy ion spectroscopy (MEIS) [15, 16]. The displacement profile of Si atoms near the interface confirmed that, while thermally grown oxide

[3] A native oxide refers to the oxide film that forms naturally on the silicon sample when exposed to air.

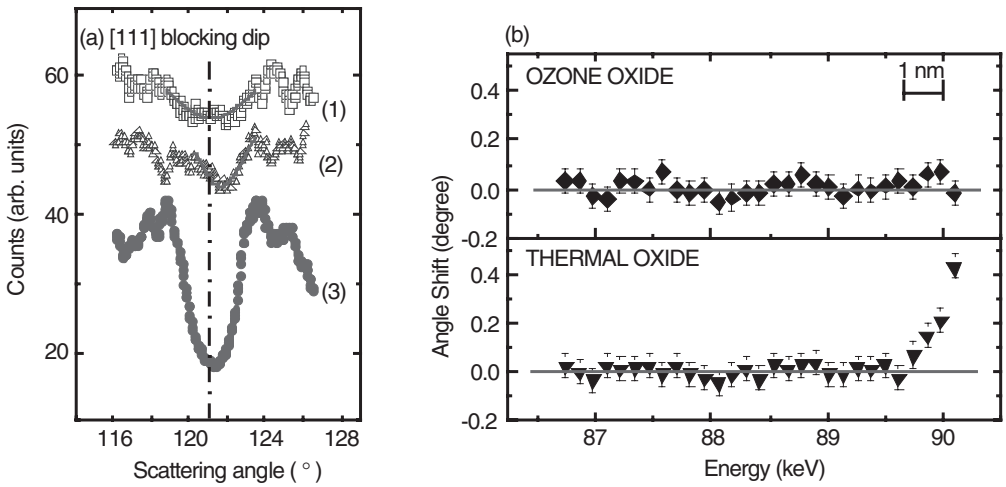

Figure 4. (a) Angular spectra around the Si blocking dips of (1) the ozone oxide and (2) the thermal oxide, and (3) the crystalline Si substrate in the [111] direction for a 4 nm oxide (parabolic fittings used to determine the dip positions). (b) Shift in blocking dip positions of the Si peak as a function of depth for the ozone oxide and thermal oxide in the [111] direction. Reprinted with permission from [16]. ©2002, Japan Society of Applied Physics.

exhibits a structural transition layer, the ozone-grown film is homogeneous even at the interface, supporting the observation of the constant HF etching rate.

In their experiments, Kurokawa *et al* [15] prepared a 3.3 nm thick oxide film by exposing Si{001} to atmospheric-pressure ozone at a substrate temperature of 375 °C, and compared it to a film of the same thickness prepared by wet oxidation at 700 °C.

Even though the XPS Si 2p spectra showed that the stoichiometry of the ozone-grown oxide is the same as that of the thermally grown oxide, the MEIS revealed differences in the displacement profile. At high incident energies, which corresponds to a penetration depth near the interface, the blocking dips of the thermal oxide shifted to a higher angle with respect to the blocking dip of bulk Si. This shift indicates the presence of a compressively strained SiO_2 layer near the interface.

In contrast, the ozone-grown oxide does not exhibit this shift, but the blocking dips near the interface keep the same angle. Thus, the oxide grown by ozone oxidation shows a negligible strain and a thinner interfacial transition layer than the thermal oxide.

The same MEIS characteristics of ozone-grown oxide were found by Chang *et al* [16] as shown in figure 4, who used slightly different processing conditions. The authors compared an ozone-grown oxide formed at 600 °C in a concentration of 3% ozone to an oxide film formed by dry oxidation (O_2) at 800 °C. Only the O_2-grown oxide formed a ≈1 nm thick structural transition layer, while the ozone-grown oxide is homogeneous even close to the interface.

Similar interface improvements were also observed by photo-oxidation methods at low temperatures. Thus, there might be two reasons for this improvement. First, the lower processing temperature might suppress diffusion effects that lead to a disruption of the oxide network (e.g. Si outwards diffusion). Second, the more reactive diffusive species of atomic oxygen might be more successful in saturating interface defects (e.g. Si dangling bonds) and so lead to a more defect-free SiO_2 network formation in the interface region. Interestingly, it was found that on a 4° tilted wafer even thermal oxidation by O_2 showed these improved interface characteristics [30]. There, it was argued that since O_2 dissociates more easily into atomic oxygens at the reactive step edges than on the planar surface, the vertical strain on the Si{001} substrate is reduced. This observation supports the second argument that the more reactive diffusion species is mainly responsible for the improved interface characteristics.

3.3.4. Si–O–Si vibrations. Since the Si–O–Si asymmetric stretching frequency is sensitive to the Si–O bond angle and bond length, it shifts towards lower wavenumbers near the interface, when strain and substoichiometric oxide are present [31, 32].

The structure of the ozone-grown oxide film near the Si/SiO_2 interface has been analysed by Fourier transform infrared spectroscopy (FTIR) [18, 12]. Even though both groups used different processing conditions and techniques to measure the thickness dependence, both found that the ozone-grown oxide exhibited different FTIR characteristics than the thermally grown oxide, suggesting improved interface characteristics.

Cui *et al* [18] oxidized a Si{001} sample in low-concentration O_3 (950 ppm in O_2 gas) at temperatures between 200 and 500 °C. They measured the longitudinal optical (LO) mode of the Si–O–Si asymmetric stretching frequency *in situ* as a function of oxidation time (increasing thickness). For short exposure times (equivalent to very thin oxide films) the LO mode was lower than the SiO_2 bulk value of 1050 cm^{-1}. As the film grew in thickness this peak shifted upwards and converged towards a frequency typical for the oxidation temperature. Higher oxidation temperatures led to an increase in the vibrational frequency, thus bringing it closer to the SiO_2 bulk value. In addition, the authors also found that ozone had a favourable effect, so that the Si–O vibrations were close

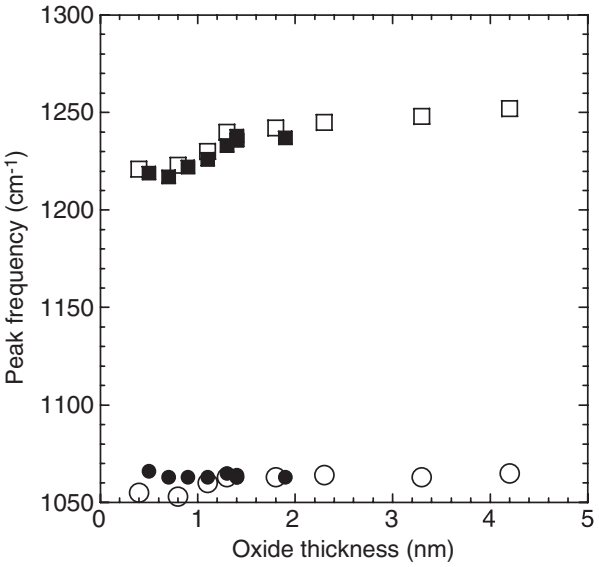

Figure 5. TO and LO mode of the Si–O–Si asymmetric stretching vibration of oxide films formed on Si{001} as a function of oxide thickness: (■) LO frequency and (●) TO frequency of ozone oxide, and (□) LO frequency and (○) TO frequency of thermal oxide. Reprinted with permission from [12]. ©2005, Japan Society of Applied Physics.

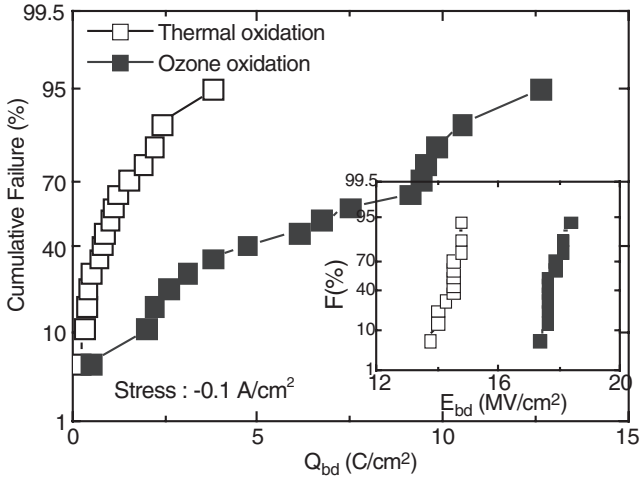

Figure 6. Charge-to-breakdown characteristics Q_{bd} under a constant current density of -0.1 A cm^{-2} of a 4 nm thermally grown (800 °C) and ozone oxide (600 °C). Inset highlights higher breakdown field strength of ozone oxide. Reprinted with permission from [16]. ©2002, Japan Society of Applied Physics.

to the bulk value even after short exposure times. Cui *et al* also performed XPS measurements to quantify the amount of suboxide, which confirmed that both higher temperature conditions and the more reactive oxidant (ozone) reduced the amount of suboxide and thus improved the interface quality.

Nakamura *et al* [12] exposed a Si{001} surface with an already present native oxide film to high-concentration O_3 (>30%) at 350 °C. In addition to the LO mode of the Si–O–Si stretching vibrations, they also measured the transverse optical (TO) mode. In order to evaluate the thickness dependence, they first grew an oxide film of 1.9 nm thickness and then etched the oxide by HF back to the desired thickness (decreasing thickness). We note, that in this method the HF etching could have an additional influence on the FTIR spectra.

While the TO phonon peak of the thermally grown oxide exhibited a red-shift by 10 cm^{-1} at a distance of 1.3 nm from the interface, the ozone oxide remained constant at 1065 cm^{-1} down to 0.4 nm thickness (figure 5). Yet, the LO phonon peak yielded for both oxides a red-shift of ≈30 cm^{-1} from its bulk value of 1250 cm^{-1}, as soon as the thickness reached values lower than 1.3 nm. While this shift of the LO mode alone is not fully understood[4], the authors have argued that the TO mode in the thermal oxide decreases, because the Si–O–Si bond angle near the interface is more distorted (≈3°) [12]. The TO stretching frequency was also calculated to exhibit a strong dependence on the Si–O bond length, as a bond length increase of just 0.01 Å lead to a red-shift of 43 cm^{-1} [32].

3.3.5. Improved reliability. The quality of the ozone-grown SiO_2 film and its Si/SiO_2 interface has also been tested for device performance [16, 33]. The lifetime of the ozone-grown oxide has been measured under electrical stress [16] and the charge-to-breakdown characteristics were found to be significantly improved (figure 6). It has been suggested that the observed strain relaxation might be responsible for the improved reliability. Alternatively, the more reactive diffusive species of oxygen radicals might be more successful in saturating any Si dangling bonds, and thus lead to a lower defect density than in the O_2-grown oxide. The ozone-grown oxide was also found to exhibit less charge trapping [16].

[4] The oxide composition and/or oxide density might be responsible for this shift.

4. Growth properties

In order to achieve a high degree of control in the silicon oxide formation by ozone, it is necessary to understand its growth characteristics.

In 1965, Deal and Grove [34] devised the now famous Deal–Grove model to describe the oxide growth in O_2 and H_2O at high temperatures. In this model, the oxidizing species is considered to undergo three stages: (I) diffusion from the bulk of the gas to the surface, (II) diffusion through the bulk oxide to the oxide–substrate interface, and (III) reaction at the interface. However, despite describing the formation of thick oxide films very accurately, this model fails to account for the formation of thin-film oxides (<20 nm) [35] and new models (considering diffusion of charged O_2, Si outwards diffusion, a reactive layer, etc) have been proposed to understand the ultrathin oxide growth by O_2 (see [36] and references therein). Interestingly, however, due to its general nature the Deal–Grove model has found validity in the case of silicon oxidation by ozone.

In most experimental studies that have investigated the relation between film thickness and oxidation time in ozone, the silicon oxide grew initially at a linear growth rate followed by a parabolic growth rate. While a linear growth rate usually indicates a surface or interface reaction-limited growth

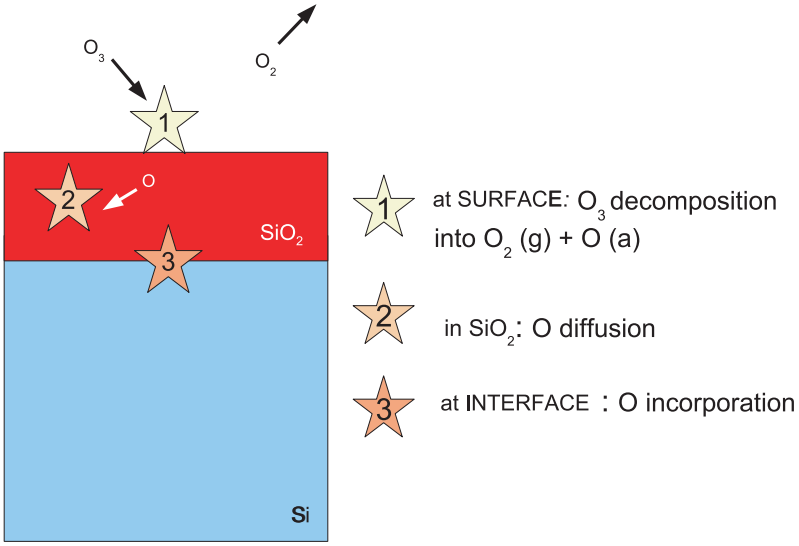

Figure 7. Schematic representation of how silicon oxide grows by oxidation in O_3.

(phenomenon III of Deal–Grove model), a parabolic growth rate suggests that the oxidation is governed by diffusion (phenomenon II). Each phenomenon can be expressed either by a linear or parabolic law with

$$x = At \tag{1}$$

$$x^2 = x_0^2 + Bt. \tag{2}$$

Here, x refers to the oxide film thickness (nm), t to the oxidation time (min), while A and B account for the linear and parabolic rate constant (nm min^{-1} and nm^2 min^{-1}), respectively. Assuming that both growth constants follow an Arrhenius behaviour, they can be expressed as $A = A_0 \exp(-E_a^A/kT)$ and $B = B_0 \exp(-E_a^B/kT)$ to describe the temperature dependence of the growth rate.

In (2) x_0 is an empirical parameter, which refers to the oxide thickness until which linear growth is observed. Thus, x_0 marks the transition from the linear to the parabolic regime and has been estimated to be ≈0.6 nm [37]. Figure 7 gives a schematic representation of the oxide growth in ozone.

4.1. Initial oxidation: adsorption

The initial oxidation stage is governed by the interaction between ozone and the silicon surface and has been studied by numerous experimental techniques, which were complemented by first-principles molecular dynamics simulations. Since it was found that the surface termination has a strong influence on the adsorption process, we will discuss the adsorption of ozone on the two most important surface terminations, the clean and hydrogen-terminated surfaces, separately.

4.1.1. Clean Si{001}. Two scanning tunnelling microscopy (STM) studies [38, 39] were performed to elucidate the initial oxidation of clean[5] Si{001} by ozone. It was observed that O_3 exposure led to the emergence of bright and dark features on the surface. However, since STM is unable to unambiguously image oxygen atoms on the silicon surface ([40] and references therein), the interpretation of these observed features differs between the two studies. While Itoh *et al* [38] related the bright features to single oxygen adsorption sites, Narushima *et al* [39] suggested these to be ejected Si adatoms. Since we are unable to solve this ambiguity, we report both interpretations, independently.

Itoh *et al* [38] identified three types of bright features, which varied in brightness and in their location relative to the dimer rows. The two most common bright features were assigned to O adatoms in the dimer and back bond sites, while the third, less frequently observed bright feature was suggested to be an O adatom in the trough region, between the dimer rows. This assignment also coincides with the adsorption sites observed by first-principles MD simulations [41] (see below).

In contrast, Narushima *et al* [39] describes the bright features as 'bumps' and 'elongated islands', and relates their origin to ejected silicon surface atoms.

Yet, both studies agree in assigning the dark features, which emerge after O_3 exposure, to an increase in surface defects ('etching'). Narushima *et al* [39] also argues that in surface areas, which have been etched to a high degree, the exposed sublayers reconstruct into new dimer rows.

To reveal the underlying 'microscopic' reaction mechanism, Fink and Jenkins [41] simulated the interaction between an impinging O_3 molecule and the clean p(2 × 2) dimer-reconstructed surface by first-principles molecular dynamics (FPMD). They found that ozone exhibited a very high reaction probability, corresponding to an initial sticking probability close to unity. Two dominant reaction pathways were observed, where O_3 dissociatively adsorbed either into a single O adatom and gas-phase O_2 (partial dissociation) or into three O adatoms (complete dissociation). The dissociation of ozone was highly exothermic and found to proceed without any activation barrier.

[5] Due to its importance in the semiconducting industry, most studies have focused on the {001} surface.

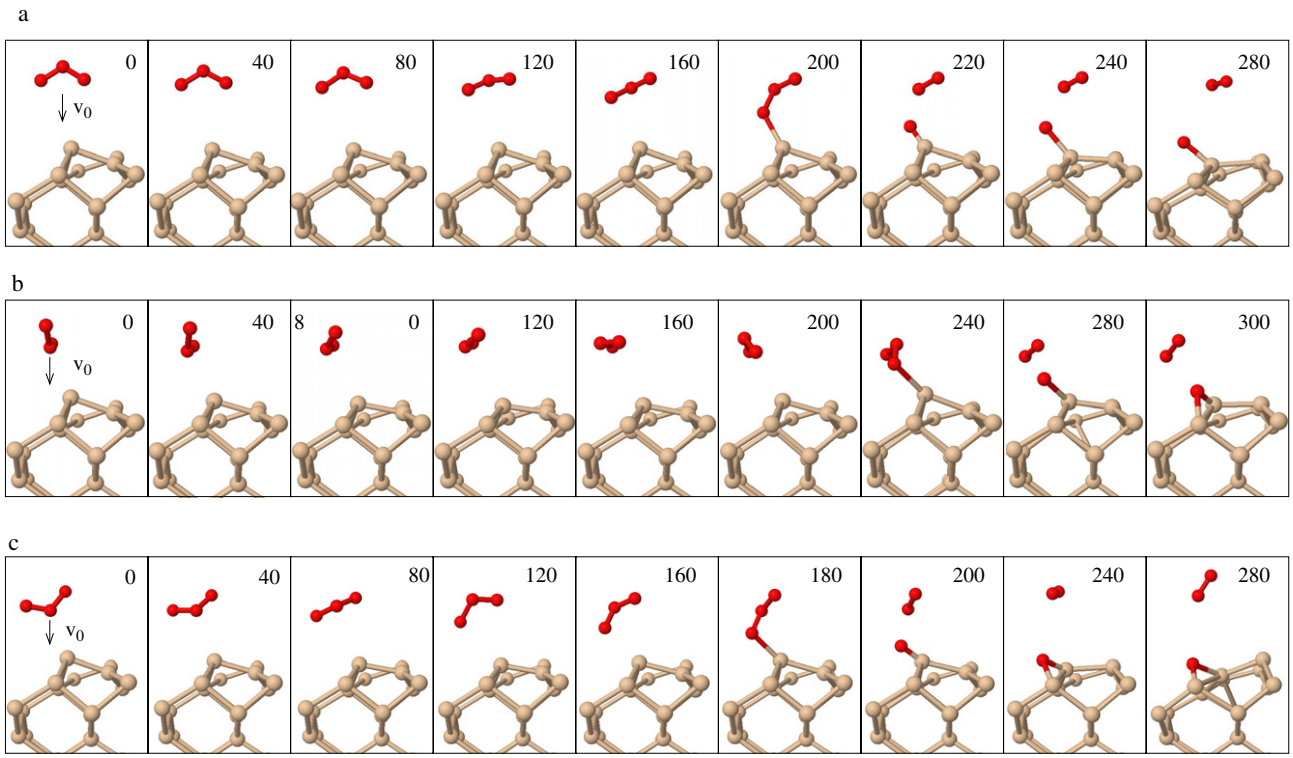

Figure 8. Molecular dynamics trajectories for O_3 approaching the Si-up dimer atom (Si^u) on the clean Si{001}. O_3 has been given a velocity of 5 Å ps^{-1} towards the surface, while all surface atoms are initially at rest. The Si^u steers the O_3 into a favourable orientation, until the molecule is eventually stripped of one of its terminal O atoms and the remaining O_2 fragment desorbs from the surface. The O adatom either stays in its initial Si^u adsorption site (a) or it relaxes into the more stable lower back bond adsorption site ((b), (c)). Time evolution given in fs. Reprinted with permission from [41]. ©2008, American Physical Society.

On the surface two reaction centres were identified, where ozone reacted with either the up (Si^u) or the down (Si^d) dimer atom of the buckled Si dimer of the reconstructed surface.

The electron-rich up dimer atom, Si^u, was found to be more reactive and displayed a pronounced steering effect onto the incoming molecule. As the trajectories depicted in figure 8 reveal, O_3 is steered by the Si^u atom into a favourable position in order that one of ozone's terminal O atoms is able to react with the surface dangling bond. After adsorbing to the Si^u atom, this O atom relaxed (in most trajectories) into the more stable dimer bond or lower back bond site.

A study of the underlying electronic structure revealed several reaction stages during the dissociation process. In particular, responsible for the surface-induced steering was the maximization of overlap between the Si^u dangling bond and the O_3 LUMO.

In contrast, the less reactive down dimer atom, Si^d, did not exhibit this steering effect on to the incoming molecule, but was able to react (depending on the incoming orientation of O_3) with either a terminal or the central O atom. By reacting with the central O atom, the molecule was even able to dissociate completely, leaving three O adatoms on the surface. Since this complete dissociation is sterically more challenging, it has been suggested to be a rare event and that the partial dissociation is the preferred reaction pathway. As mentioned earlier, the products of partial dissociation coincide with the assignment of the STM data of Itoh *et al* [38], that single O atoms occupy the back bond and the dimer bond.

In comparison to O_3, regular O_2 exhibits a much lower sticking probability, since the adsorption of O_2 on Si{001} proceeds only via a narrow dissociation pathway [42]. Therefore, the initial oxidation by O_3 proceeds much faster and at much lower temperatures than by O_2.

The reason why O_3 exposure leads to the creation of surface defects even at low temperatures was also investigated [41]. Previously, the activation barrier for SiO ejection was found to have a strong dependency on the oxidation state of the Si atom [43], so that the barrier for ejection of a singly oxidized Si atom, Si^{1+}, is much lower (at around 2 eV) than for higher oxidized Si atoms (Si^{2+}, Si^{3+}, and Si^{4+}).

Putting this observation in the context of the oxidation by ozone, the hot O adatom from the partial dissociation of ozone has a large enough kinetic energy to enable a SiO ejection of the singly oxidized Si atom [41]. This SiO ejection mechanism is able to explain the microscopic origin for the experimentally observed increase in defects during ozone exposure [38, 39]. In contrast, the dissociation of O_2 leads to the formation of a doubly oxidized Si^{2+} species; due to its additional Si–O bond, this species is much stronger bound to the surface and therefore exhibits a much higher activation barrier of around 4 eV for SiO ejection [43].

Thus, while oxidation in O_2 results in etching only at the specific thermodynamic conditions of high temperature and low pressure, also referred to as the 'active oxidation' regime,

the dissociation of O_3 increases the likelihood for an early etching event even at low temperatures.

4.1.2. Hydrogen-passivated Si{111} and Si{100}. The hydrogen-terminated silicon surfaces, which are rather inert with respect to O_2, were found to be readily oxidized by ozone even at low temperatures [44, 45]. This fact is significant, since it is common practice in industry to protect clean silicon surfaces with a passivating coverage of hydrogen prior to controlled oxidation.

Even though the sticking probabilities of both ozone and molecular O_2 were reduced with increasing hydrogen coverage, at a full hydrogen coverage only O_3 was still able to oxidize Si{111} at the processing temperature of 70 °C [44], as shown in figure 9.

Nevertheless, compared to adsorption on clean Si{111}, O_3 exhibits a considerably lower sticking probability on the hydrogen-terminated surface. Here, the initial rate of oxide formation has been estimated to be reduced to one tenth at low temperature conditions (50 °C) [45].

A similar behaviour was observed in the oxidation of hydrogen-terminated Si{001}. By measuring the stress evolution during oxidation by ozone, it was revealed that the hydrogen-terminated surface exhibited a rate of initial stress increase that was lower than for the clean surface [46]. This was linked to the effect that surface hydrogen would lower ozone's initial sticking probability. Nevertheless, after long enough exposure, the stress of both clean and H-terminated surface saturated at almost the same value and became by ≈ 0.3 N m^{-1} more compressive with respect to the sample prior to oxidation. This suggests that the later oxidation stage is independent of the surface termination.

First-principles molecular dynamics simulations have provided new insights into the microscopic surface reaction [47, 48]. The simulations confirmed that independent of the crystallographic orientation of the surface ({001} or {111}) a termination by hydrogen exhibits a repulsive interaction with ozone, and thus lowers ozone's sticking probability.

Nevertheless, the FPMD simulations revealed several low-barrier oxidation channels [48], where ozone succeeded in the direct oxidation of a Si–Si bond. Through a partial dissociation mechanism, where the O_2 fragment desorbed, one of O_3's terminal O atoms was inserted into the dimer bond, back bond, or subsurface bond, which released a heat of adsorption of 5.57, 4.97, or 4.81 eV, respectively.

In addition, in the interaction between ozone and surface hydrogen an intriguing radical-mediated adsorption mechanism was observed [47], which allowed ozone to oxidize the Si–H bond itself (figure 10). Here, ozone was able to abstract a surface hydrogen atom and form a short-lived $HO_3^{\bullet}$ radical. Due to the close proximity of an unpaired silicon surface dangling bond, which was created through the H-abstraction, the $HO_3^{\bullet}$ species exhibited only a very short lifetime of ≈ 0.2 ps. As summarized in figure 11, a variety of dissociation channels was observed, which independently led to the same reaction product of gas-phase O_2 and a surface hydroxyl –OH.

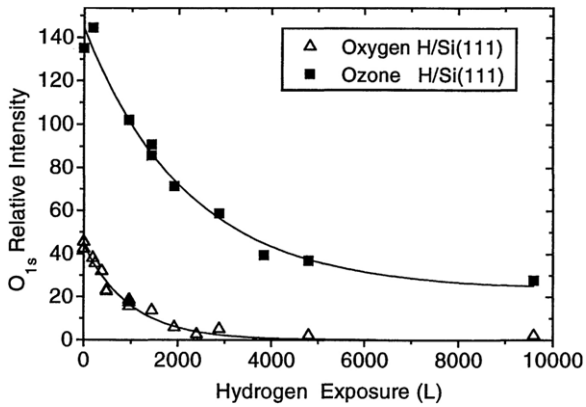

Figure 9. XPS signal of O 1s intensity on Si{111} with various hydrogen coverages after 4 L of ozone or molecular oxygen exposure (concentration of O_3 >80%, temperature at 70 °C). Reprinted with permission from [44]. ©1995, Japan Society of Applied Physics.

Even though this abstraction mechanism was found to be sterically challenging, it exhibited only a low activation barrier of 0.04 eV [48] and was found to proceed in an 'autocatalytic' way [47]. Since the surface hydroxyl is able to form an H bond to one of O_3's terminal O atoms [47, 49], the sticking probability of ozone is increased, which facilitated not only the Si–H oxidation (as depicted in figure 10(d)) but also the Si–Si oxidation.

Assuming that both Si–Si and Si–H oxidation take place, it is of interest to investigate how the oxidation proceeds after the initial stage. Interestingly, first-principles calculations [48] show that an increasing O coverage lowers the probability for the oxidation of the Si–H bond, since with increasing oxidation state of the Si atom, its Si–H bond increases in strength, too. Thus, only when abstracting an H atom from a Si atom with zero (Si^0) or one oxygen bonding partner (Si^{1+}) is the formation of the $HO_3^{\bullet}$ reaction intermediate exothermic. In contrast, for the higher oxidized Si^{2+} and Si^{3+}, it is energetically more favourable for the H atom to stay bound to the oxidized Si atom than to bind to the O_3. Thus, if the oxidation of the Si–H bond indeed takes place via the suggested mechanism, the transformation of Si–H into Si–OH would saturate soon after the initial oxidation stage.

Next, we relate this theoretical model that ozone not only oxidizes the Si–Si, but also the Si–H bond to available experimental data. We note that a direct oxidation of the Si–H bond has been already experimentally confirmed for another highly reactive oxidation gas, namely atomic O. Ikeda *et al* [50] exposed the H-terminated Si{001} to oxygen plasma and observed a sharp increase in the Si–OH stretching vibrations. The O atoms were simultaneously inserted into the Si–H and Si–Si bond, of which the latter proceeded faster. Nevertheless, we find that the Si–H oxidation by ozone has not been fully investigated by experiments yet.

Cui and Takoudis [51] have studied the initial oxidation of H-terminated Si{001} by O_3 (950 ppm)/O_2 gas at temperatures between 50 and 300 °C. The activation barrier for the initial oxidation regime was very low and estimated to be less than 0.05 eV.

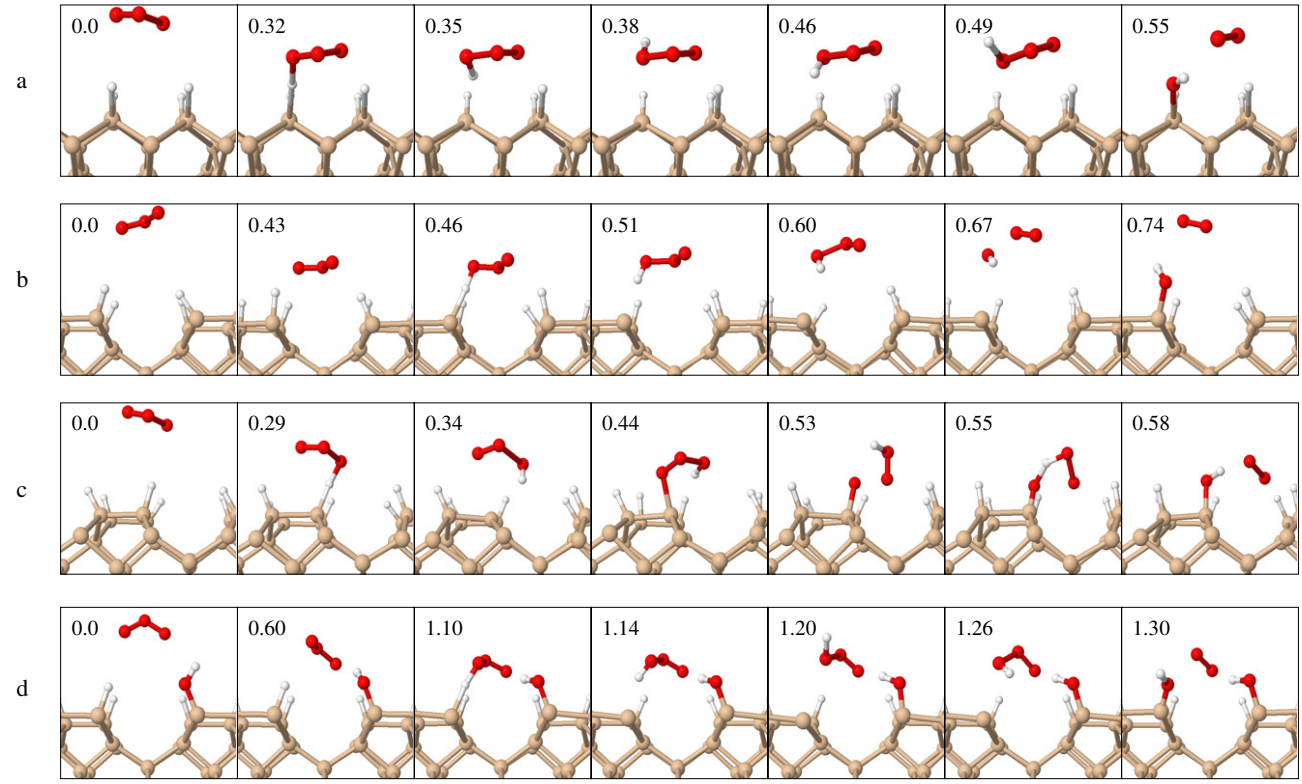

Figure 10. Molecular dynamics trajectories revealing how O_3 abstracts surface hydrogen to form Si–OH. Trajectories (a), (b) and (c) describe three different dissociation pathways for $HO_3^{\bullet}$. Trajectory (d) describe in the presence of pre-existing surface hydroxyl. For visualization purposes the viewing direction for trajectory (a) is chosen orthogonal to that of the other trajectories. Time given in ps. Reprinted with permission from [47]. ©2008, Elsevier.

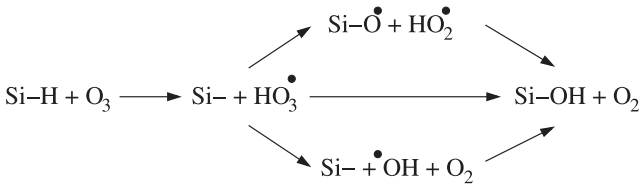

Figure 11. Reaction scheme for initial oxidation of the hydrogen-terminated Si surface via the $HO_3^{\bullet}$ intermediate.

A change in the surface polarity was observed, as the H_2O contact angle decreased upon oxidation, as the surface changed from being hydrophobic (H-terminated) to hydrophilic (oxide). The contact angle of the surface oxidized in ozone had a lower H_2O contact angle than the sample oxidized in O_2, suggesting a lower H coverage on the ozone-oxidized sample.

The same authors also used Fourier transformed infrared (FTIR) spectroscopy during O_3 exposures, but did not investigate the frequency range where O–H vibrations would occur [51]. Instead, three groups of vibrational bands were observed in the recorded frequency range between 1500 and 3300 cm^{-1}.

Two groups, which lowered their intensity after O_3 exposure, were located at 2850–2961 and 2086 cm^{-1}, and were linked to the removal of carbon contaminants and the removal of surface hydrides, respectively. The lowering of the hydride (Si–H) signal, however, could also be explained by transformation into hydroxyls (Si–OH).

Interestingly, at temperatures below 290 °C a phonon peak emerged at 1727 cm^{-1}, which was suggested to be either related to a chemisorbed ozone species or to a surface carbonyl (>C=O). Since DFT simulations [47, 41] have shown that O_3 is not able to form an intact adsorbed species, this vibrational feature is most likely linked to the oxidation of the hydrocarbon contaminants.

An indication that surface hydrides are not completely removed is given by the following experiments. If ozone exposure led to the complete removal of the surface hydrides, it would be expected that after O_3 exposure the surface would be oxidized by O_2. Yet, consecutive exposure of a hydrogen-terminated Si{111} surface to O_3, O_2, O_3, and O_2 revealed that the oxide film thickness only increased during O_3 gas exposure, and did not change during O_2 exposure, as shown in figure 12 [29]. The authors suggested that the surface would keep its H-termination, which hinders oxidation by O_2. Alternatively, since surface hydroxyls exhibit the same repellent behaviour as surface hydrogens with respect to O_2, the oxidation of the Si–H could also explain the observation that O_2 was not able to oxidize the surface after O_3 exposure.

Interestingly, temperature programmed desorption (TPD) experiments [52] showed that a lower amount of H_2 desorbed from the surface after ozone oxidation. This suggests that O_3 indeed interacts with the surface hydrides, either by indirect hydrogen removal (e.g. the exothermicity of the oxidation leads to a local heating effect, which excites the Si–H bond into

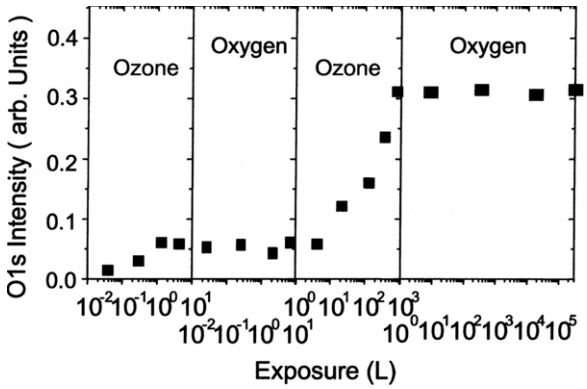

Figure 12. Change of O 1s intensity with exposure of H-terminated Si{111} sample to ozone and molecular oxygen gas. The gas exposure was performed in order of O_3, O_2, O_3, O_2 exposure. Reprinted with permission from [29]. ©2000, Elsevier.

higher vibrational modes, and so induces H_2 desorption) or by transformation of Si–H by oxidation into Si–OH. Since neither the signal of H_2O nor of any other OH-related desorption species were investigated by TPD, the latter cannot be ruled out.

Thus, we find that in order to clarify how ozone exposure affects the hydrogen termination (e.g. does ozone create surface hydroxyls as suggested by the simulations?), additional experiments are necessary. For example, IR measurements during the initial oxidation stage could probe the frequency range where hydroxyl vibrations occur (typically at $\approx$3750 cm^{-1}).

Nevertheless, the later oxidation stage appears to be governed by diffusion, where silicon's surface termination appears to play a minor role.

4.2. Transition: O_3 reacts with partially oxidized Si{001}

Already in their early studies, Kazor and co-workers [26] concluded that the inward diffusion of atomic oxygen through the SiO_2 film would be the rate-determining process in the later oxidation stage. In order to understand the transition from the initial adsorption to the later growth mode, FPMD simulations have investigated the interaction between O_3 and an increasingly oxidized Si{001} [48].

The simulations revealed that with increasing O coverage ozone's sticking probability was reduced. Whereas on the clean surface each incoming molecule reacts with the surface, the preadsorbed O atoms exhibit a repulsive potential on the ozone. Therefore, in the vicinity of the O adatoms, ozone was repelled and either desorbed back into the gas phase or managed to get into the vicinity of an unoxidized Si–Si bond, where ozone would react. Here, the partial dissociation of ozone dominated, so that the Si adsorption sites were gradually filled by single oxygen atoms, while the O_2 fragments desorbed.

O_3 preferentially reacted with surface Si atoms which had a lower oxidation state [48]. This led to a uniform oxidation, which has been experimentally observed by atomic force microscopy (AFM) [53]. The experiments confirmed that room temperature oxidation of Si{001} by ozone proceeded in a homogeneous layer-by-layer mode, where the step-terrace morphology of the clean surface was preserved both on the oxide surface and also at the SiO_2/Si interface.

Nevertheless, the simulations observe a clear transition in the oxidation rate. After more and more Si adsorption sites are filled, the rapid dissociative adsorption mechanism eventually gets blocked and only resumes when O atoms diffuse from the surface into the subsurface [48]. Such a diffusion mechanism, which leads to the oxidation of a Si–Si subsurface bond and the formation of a fully oxidized Si^{4+}, is depicted in figure 13.

In brief, upon dissociative adsorption of a single O onto Si^{3+}, a Si subsurface dangling bond is created. To saturate this defect, an O atom hops from a neighbouring surface site and occupies this subsurface site. This hopping itself creates a surface dangling bond, which is filled by subsequent diffusion of an O atom. All three events (creation of dangling bond, O hopping, O hopping) happen within a very short time period (<500 fs). Analogue diffusion reactions are expected to play an important role in the transition from the initial adsorption to the later oxidation stage.

Having obtained insight into how ozone reacts with a lightly oxidized silicon surface, we now turn to the full oxide growth.

4.3. Later oxidation: diffusion

In table 2 we provide a comparison[6] of the oxide growth characteristics by ozone as experimentally observed.

It becomes clear that the oxidation kinetics depend on many parameters, as for example the reported values for the diffusion barrier show a large variation with values between 0.14 eV $< E_a <$ 0.80 eV. Interestingly, a similar variation in the activation energy has been observed for the plasma oxidation of silicon, where the space charge, which was different in each experimental setup, was found responsible for this variation [55].

In the oxidation by ozone, effects of charge transfer are expected to play an equivalent role in influencing the diffusion rate. This is because the diffusion barrier of the O atom, which diffuses through the oxide, exhibits a strong dependence on its charge. By looking at the results of first-principles calculations [56, 57] the diffusion barrier for neutral O^0 and negatively charged O^- are revealed. The neutral species exhibits a much higher barrier of 1.3 eV [56], while charge transfer lowers the barrier of O^- to 0.27 eV [57]. The latter value is in much better agreement with the activation energies for the diffusive species related to ozone oxidation.

Of the experimental setup, the generator type, the O_3 concentration, and the total pressure in the chamber[7], exhibit a strong influence of the growth characteristics, as table 2 highlights. These experimental conditions determine the supply of ozone to the surface.

[6] Such a comparison has already been conducted by Narushima *et al* [54], which we have expanded here to include studies published after 2001.

[7] Since the heating system (gas-phase heating or sample-only heating) is also expected to affect ozone's lifetime, gas-phase heating is explicitly labelled in the table.

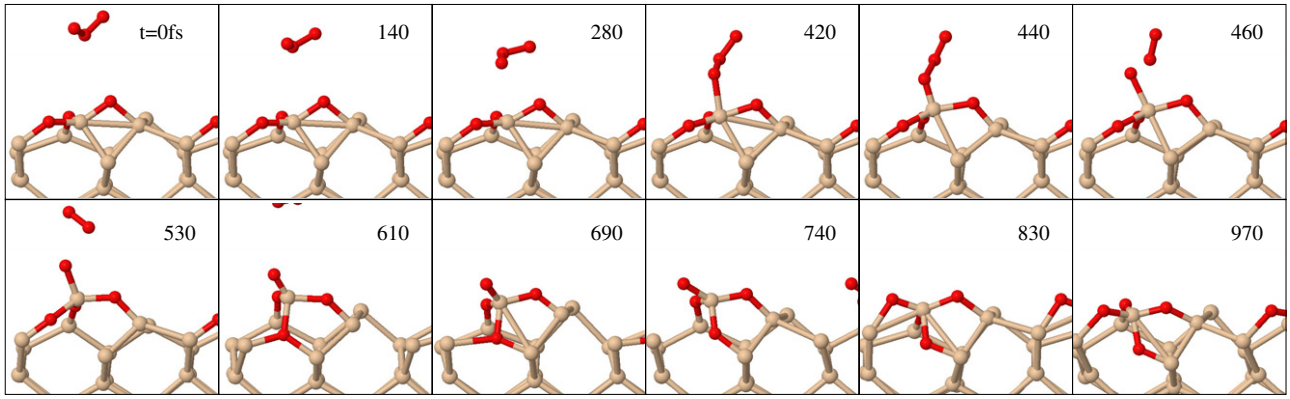

Figure 13. Molecular dynamics trajectory of O_3 impinging on a partially oxidized Si{001} (0.75 ML O coverage). O_3 has been given a velocity of 5 Å ps^{-1} towards the surface, while all surface atoms are initially at rest. The O_3 is able to bring one of its terminal O atoms into the vicinity of the Si^{3+} site, which initiates the adsorption of a single O adatom and the subsequent migration of an O atom from the back bond into the subsurface site. Time evolution given in fs. Reprinted with permission from [48].

Table 2. Growth characteristics of silicon oxidation by ozone. Abbreviations of generator types are presented in table 1. *A* and *B* are linear and parabolic rate constant.

Year	Authors	Sample	Generator	O_3 conc.	T (°C)	Mechanism	Rate constant, growth rate	E_a (eV)
1989	Chao *et al* [7]	Si{001}, clean	UV/O_2	2.25 ppm	700–950		6.2 nm after 140 min at 700 °C	
2000	Cui *et al* [18]	Si{001}, H-pass.	UV/O_2	950 ppm	125–530[a]	2 linear regimes (fast < 5 min < slow)	2.2 nm after 20 min at 500 °C 2.6 nm after 75 min at 500 °C	0.13 (fast) 0.19 (slow)
1993	Kazor and Boyd [9]	Si{001}, H-pass.	BDO	3–4%	400–550	parabolic (up to 4 h)	$B = 2.7$ nm^2 min^{-1} at 500 °C	0.80
1994	Kazor *et al* [26]		BDO	3–4%	600–1200	parabolic	$B = 6.6$ nm^2 min^{-1} at 800 °C	0.22
2002	Narushima *et al* [54]	Si{001}, H-pass.	BDO	7%	700	parabolic	$B = 40.2$ nm^2 min^{-1} at 700 °C	
2000	Nakamura *et al* [58]	Si{001}, clean	OJG	80% $p < 10^{-3}$ Pa	RT-700	Linear (0.4–1.2 nm)	1.0 nm after 90 min at 600 °C	
2001	Maeda *et al* [53]	Si{001}, clean	OSG	30% $p = 10^5$ Pa	RT	layer-by-layer growth	1.0 nm after 270 min at RT	
2002	Nishiguchi *et al* [33]	Si{001}, H-pass.	OJG	93% $p = 900$ Pa	260–830[a]	Parabolic (3–11 nm)	6.0 nm after 3 min at 600 °C	0.32 (above 400 °C)
2005	Koike *et al* [59]	Si{001}, H-pass.	OSG	25% $p = 1100$ Pa	340–625	Parabolic (1–5 nm)	3.5 nm after 3 min at 625 °C	0.52
2001 (2002)	Nishiguchi *et al* [37] [60]	Si{001}, H-pass.	PLD	80%	RT–550	linear (<0.6 nm) parabolic (>0.6 nm)	1 nm synthesized by 1000 laser shots at 350 °C	0.0[b] 0.14 (0.17)
2005	Tosaka *et al* [22]	Si{001}, H-pass.	UV/O_3	93% $p = 200$–800 Pa	70–300	linear (<5 min) Parabolic (>5 min)	$A = 0.5$ nm min^{-1} at 70 °C $B = 0.1$ nm^2 min^{-1} at 70 °C 3.6 nm after 10 min at 70 °C	0.025 0.14

[a] Gas-phase heating.
[b] Kinetic energy of $O_3 \approx 0.4$ eV.

An additional impact on the growth rate, which we only mention briefly here, might come from the sample's type of doping (n-or p-type) and dopant concentration, which is expected to facilitate the charge transfer into the diffusion species. Yet, since the majority of samples presented in table 2 were of p-type, with a resistivity in the order of 5 Ω cm, it is difficult to quantify this impact. In any case, compared to the other factors this influence is expected be negligible.

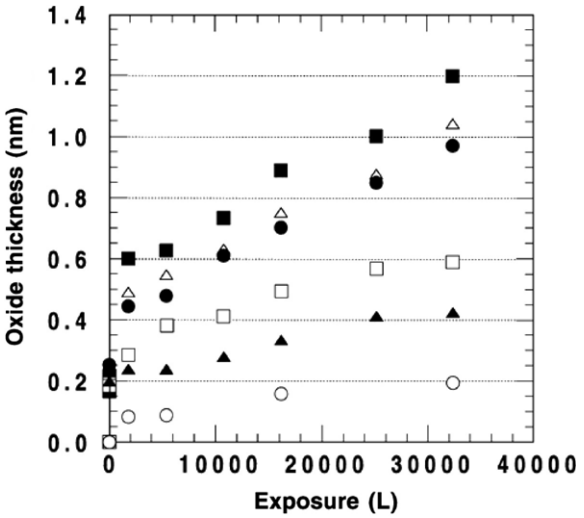

Figure 14. Growth kinetics during initial oxidation of Si{001} by ozone at low pressure conditions: the fast initial adsorption process is followed by ultrathin film growth. Yet, at substrate temperatures below 550 °C, the film saturates in thickness. Gas-phase pressure of ozone at 8×10^{-4} Pa with substrate temperatures at (○) RT, (▲) 300, (□) 500, (●) 550, (△) 600 and (■) 700 °C. Reprinted with permission from [58]. ©2000, Japan Society of Applied Physics.

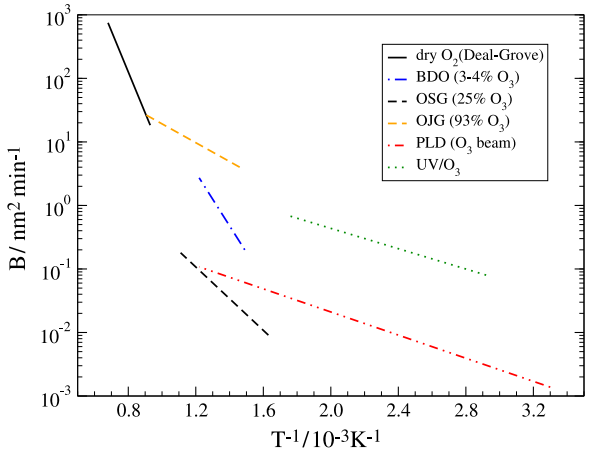

Figure 15. Comparison of parabolic rate constant B. Oxidation in ozone for different ozone supply: BDO barrier discharge ozonizer with 3–4% concentration of ozone (pressure in chamber, $p = 10^5$ Pa) [9], OJG ozone jet generator with 93% ($p = 900$ Pa) [33] and OSG ozone silica generator with 25% ($p = 1100$ Pa) [59], PLD pulsed laser deposition (one laser shot per second) [60]. As reference Deal–Grove model, parabolic rate constant of oxidation in dry O_2 [34] (valid for oxide thickness >20 nm).

In their pioneering work, Chao *et al* [7] found that, despite its low concentration, the presence of O_3 enhanced the oxide growth rate significantly. In the temperature range between 700 and 950 °C the oxidation in the UV-generated O_3 (2.25 ppm)/O_2 mix gas was up to 96% faster than in pure O_2. However, for thicker films and higher temperatures, where O_2 alone exhibits fast oxidation rates, this relative growth enhancement in the O_3/O_2 mix gas decreased.

Cui *et al* [18] also used a UV-based O_3 generator (UV/O_2) producing an ozone concentration of 950 ppm in the O_2 gas. By measuring the *in situ* IR intensity during the exposure of mixed O_3/O_2 and pure O_2 gas two linear oxidation regimes were identified for the growth of ultrathin oxide films (<3 nm). For O_3/O_2 the fast initial oxidation regime exhibited an activation barrier of 0.13 eV and changed after approximately 5 min exposure into a slower oxidation (up to ≈30 min exposure) with an estimated barrier of 0.19 eV. In comparison, oxidation in pure O_2 yielded higher barriers of 0.20 and 0.36 eV for the two oxidation regimes respectively.

In contrast to cold-wall processing in this setup a heating lamp was used, which thermally excites the gas-phase ozone and thus affects its lifetime. Therefore, it was found that at temperatures above 500 °C the ratio between the oxidation rates of O_3/O_2 and pure O_2 actually decreased. *In situ* FTIR measurements confirmed that at 530 °C a large proportion (≈75%) of the inlet ozone decomposed at steady state, while at 125 °C only a few ozone molecules (≈9.5%) decomposed. Since atomic O would have a much shorter lifetime, the decomposition of O_3 forms O_2, which is less reactive in the oxidation process. Based on a first-order reaction, the activation energy for ozone dissociation was estimated to be ≈0.17 eV. Since this activation barrier was very close to the barrier of the slower oxidation regime, the dissociation of ozone was suggested to be the rate-limiting step in this oxidation process [18]. This would also explain the observation of a linear, instead of a parabolic (diffusion-limited) growth.

Despite these low ozone concentrations in the O_2 gas (<4%), the oxidation is clearly governed by the presence of ozone, which supplies the more reactive oxygen atoms to the surface. Therefore, the value of the parabolic rate constant B was found to increase linearly with the ozone gas partial pressure (2–7%) [54].

At high ozone concentrations but at low pressure conditions ($p < 10^{-3}$ Pa), even though the O_3 concentration is close to 100%, the partial pressure of ozone and thus the oxidation rate is nevertheless low. This became particularly apparent in a study of the oxidation of clean Si{001} by a highly-concentrated ozone gas at very low pressure conditions ($<10^{-3}$ Pa, O_3 generator: OJG) [58]. Initially, the oxidation proceeded in accordance with Langmuir kinetics, which is typical for adsorption. Nevertheless, in the later oxidation stage, the oxide growth either saturated or followed linear kinetics, depending on the oxidation temperature (figure 14).

If the substrate was heated to temperatures ⩽500 °C, the oxide thickness saturated after an exposure of 90 min at a thickness of 0.2, 0.4, or 0.6 nm for temperatures of 30, 300 or 500 °C, respectively.

On the other hand if the oxidation temperature was ⩾550 °C, the film did not saturate, but the growth mode changed into linear kinetics as soon as the oxide reached a thickness of 0.6 nm. Thus, after 90 min exposure a 1.0 nm or 1.2 nm thick film was formed for a temperature of 550 °C or 700 °C, respectively. This transition at 0.6 nm describes the change of growth mode from adsorption to thin-film growth [58]. Yet, in this sub-2 nm regime, the growth follows a linear behaviour, which suggests that the oxidation is reaction-limited, rather than diffusion-limited (which should lead to

parabolic growth). We think that due to the low pressure of O_3, there is a shortage of ozone molecules at the gas/oxide interface, which limits the growth.

To account for the growth saturation at temperatures below 500 °C, the decomposition rate of ozone might be too low.

Similarly, in pure O_3 gas, but under slightly higher pressure conditions ($p > 250$ Pa, OSG), it was found that the oxidation rate decreased significantly at temperatures below 400 °C [33]. This was linked to the low decomposition rate of O_3, so that less O atoms could react with the surface. In order to supply reactive O atoms and guarantee a fast oxidation rate even at temperatures below 400 °C, alternative methods are necessary, including the pulsed laser deposition (PLD) and UV-excited ozone (UV/O_3) method.

Nishiguchi *et al* [37, 60] found that the oxidation rate by a hyperthermal ozone beam (PLD) was independent of the substrate temperature up to a thickness of ≈0.6 nm. Since the ozone molecules had a very high translational kinetic energy (between 0 and 2 eV) they could easily overcome any activation barrier related to the initial oxidation. Yet, at a thickness larger than 0.6 nm the growth mode changed from being linear into the parabolic regime, indicating that the oxidation kinetics became diffusion-limited. Thus, instead of being a surface reaction, which is influenced by the kinetic energy of the incoming ozone, the diffusion of the oxygen species through the growing oxide film was influenced by the substrate temperature. The activation barrier for this parabolic growth regime was estimated to lie between 0.14 [37] and 0.17 eV [60].

In addition to the higher reactivity, in this method the supply of ozone molecules is highly controllable. Tuning the repetition rate of the laser pulse gives precise control over the oxidation rate: e.g. 1000 laser shots formed a 1 nm thick oxide film at 350 °C, which depending on a repetition rate of 1 or 10 Hz either takes 1000 or 100 s.

Alternatively, UV-excited O_3 also allowed oxidation at room temperature. Ozone has a strong absorption band between 220 and 310 nm, also referred to as the Hartley band. In this band the photodissociation of ozone results in a quantum yield of unity in the reaction products of O_2 ($^3\Sigma$) and O(^{1}D). Thus, while thermal decomposition of ozone results in oxygen atoms in the ground state O(^{3}P), the decomposition of ozone by UV-light leads to oxygen atoms in the more reactive O(^{1}D) state. It has been suggested that the oxygen atoms in this excited O(^{1}D) state [61, 25] are responsible for the increased reactivity of UV-light excited O_3.

Tosaka *et al* [25] analysed the O_3 density after UV-light irradiation and discussed the change in the O(^{1}D) density. They concluded that, even though the O(^{1}D) atoms have only a very short lifetime (≈1 μs at $p = 200$ Pa) due to their high density this excited O species was indeed supplied to the surface in a pulse like fashion with each laser shot [25].

Yet, the UV irradiation also affects the silicon sample. Upon direct UV illumination, even though no defects are created, the surface temperature increases by up to 50 °C [17, 25]. In addition, the electron population in the UV-illuminated oxide is expected be higher than the thermal equilibrium concentration, which promotes electron transfer into the diffusion species and affects the diffusion rate.

It was found that the growth rate during UV/O_3 oxidation did not follow the parabolic law, but became slower as the oxide thickness increased [5]. To account for this behaviour it was argued that the quenching of O(^{1}D) to O(^{3}P) during the diffusion in the oxide would be responsible for these slower oxidation kinetics [61]. However, while the spin assignment of O(^{3}P) as ground state for atomic oxygen in the gas phase is correct, in the oxide the oxygen atom interacts with the lattice and binds temporarily to neighbouring Si atoms. Through this interaction, the spin state of the atomic oxygen relaxes almost immediately into its ground state. In addition, charge transfer into the diffusing oxygen atom has to be considered, which alters its electronic configuration from O^0 to O^-. Instead of a spin quenching, we suggest to consider a reduction in charge transfer for this decrease in oxidation kinetics: with increasing oxide thickness, the probability decreases for electrons to tunnel from the Si valence band into the SiO_2 conduction band.

Finally, to visualize the influences on the growth characteristics, plots of the parabolic rate constant of representative studies are shown in figure 15. At temperatures between 350 and 800 °C common O_3 generator types (including BDO, OJG, and OSG) offer a fast oxidation of silicon, whereas at temperatures below 300 °C alternative methods are necessary. Here, because of the low thermal budget only the PLD or UV/O_3 methods provide a fast oxidation, which is facilitated by either the high kinetic energy of the O_3 beam or by the UV-excitations.

Figure 15 highlights again the strong influence of the generator type on the oxidation rate. At temperatures between 350 and 800 °C the growth rates between the three generator types (BDO, OJG, OSG) differ by several orders of magnitude. In this comparison, the ozone jet generator (OJG) [33] offered the fastest growth rate. With the highest ozone concentration of over 93% and a total pressure of 900 Pa, it supplied ozone at a partial pressure of 830 Pa. In contrast, the barrier discharge ozonizer (BDO) [9], even though it supplied ozone at a higher partial pressure (4000 Pa, 4% at 10^5 Pa), resulted in a slower oxide growth. As a possible explanation one could consider the influence of O_2, which, at a concentration of 96%, constitutes to the majority gas and might block the fast oxidation channels of O_3. In this temperature range the slowest growth rate was given by the ozone silica generator (OSG) [59]. Although the concentration of ozone was fairly high at 25%, the total gas pressure was low at 1100 Pa, which resulted in the lowest partial pressure of all three studies ($p_{O_3} = 270$ Pa).

We conclude that the O_3 concentration and the total pressure conditions, both of which are directly linked to each generator type, influence the growth rate of the oxide significantly.

4.4. Growth and improved interface

In an effort to understand how the growth in ozone leads to improved interface characteristics, the stress evolution during the oxidation of clean Si{001} by O_2 and O_3 has been studied by the optical cantilever bending method [39]. During exposure to O_3 a monotonic increase towards the compressive stress side is observed, which saturates at a value of 0.33 N m^{-1} while the film thickness saturates at 0.6 nm.

In contrast, during exposure to O_2 at the same temperature and pressure conditions (room temperature, 0.2 Torr) the stress only increased marginally to 0.002 N m^{-1}. However, the SiO_2 film thickness after this O_2 exposure is not reported and it seems highly likely that at these low temperature and low pressure conditions, O_2 shows little to no reaction with the silicon surface. Therefore, the reported differences in the stress evolution during O_2 and O_3 exposure are not necessarily linked to the oxidation mechanism but might only reflect the higher reactivity of O_3.

More interesting is the comparison with the stress evolution during plasma oxidation, which gives a very different profile [39]. In contrast to ozone's monotonic increase in compressive stress, plasma oxidation displays three stress stages, namely tensile-compressive-tensile. This complicated profile was linked to the Si{001} surface structure, since it disappeared after the surface structure was destroyed by Ar bombardment [62].

From STM experiments ozone exposure was found to etch the surface and thus to affect the surface structure. This roughening of the surface was argued to be responsible for the release in tensile stress, which would allow a stress-free growth [39].

Despite this ozone-induced etching, which leads to a roughening of the surface, AFM experiments confirmed that the surface terraces of the ozone oxide film were nevertheless smooth [53]. While for a thickness of 1.0 nm the native oxide exhibited a root-mean-square value of the measured height >0.20 nm, the ozone oxide's RMS value was much smaller. The RMS of the ozone oxide was 0.10 nm, which was comparable to thermally grown oxide (O_2/900 °C). Interestingly, further oxidation led to a flattening of the surface, since 1.0 nm thick ozone oxide had a slightly lower RMS (0.05 nm) than a 1 ML ozone oxide (0.07 nm). This could indicate that etching is induced only during the initial oxidation stage (also refer to our discussion how the oxidation state of Si affects its etching barrier, see 4.1.1).

In addition, the initial oxidation of clean Si{111}7 × 7 by O_3 and O_2 was studied via second harmonic generation (SHG) [63]. Since this technique is particularly sensitive to resonances of dangling bond surface states and strain, it is interesting to note that oxidation in O_2 and O_3 resulted in different SHG signals.

Initially, the SH intensity exhibited a fast decay for both oxidants, which was related to the saturation of dangling bonds by the adsorption of oxygen. However, while O_2 exposure (at RT and 400 °C) after reaching a minimum resulted in a slow gradual rise of the SHG signal, the signal during O_3 exposure (at RT), not only dropped to a lower minimum, but did not gradually rise. Instead, the SHG intensity of oxidation in O_3 exhibits a significant temporary increase between 5 and 10 Langmuir exposure, before it gradually decreases again. Ozone's SHG signal might reflect the temporary increase in etching-induced surface defects or indicate a favourable strain release, which takes place already in the early oxidation stage of ozone.

Nevertheless, the role of this ozone-induced etching in the formation of a less-strained interface, is not clear. We think that the most likely origin for the improved interface characteristics, is related to ozone's diffusion species. In the oxidation by ozone the diffusion of the more reactive O atom, in contrast to a diffusion of O_2, allows a structural relaxation of the SiO_2 network near the interface. Further studies are necessary, however, to shed light on the interface formation.

5. Outlook: oxidation in ozone beyond silicon

Having extensively discussed the oxidation of silicon by ozone, we now give a brief overview of how ozone has been used in the fabrication of other oxide materials, most notably in the growth of metal oxides.

5.1. Semiconductor materials

Crystalline SiGe was successfully oxidized in O_3 at low temperatures [64]. Similar to the oxidation in silicon, the growth followed a parabolic behaviour with an activation barrier of ≈0.12 eV, which is slightly lower than in pure Si. With increasing temperature (125–530 °C) the Ge content in the oxide decreased and also the suboxide (Si^{1+}, Si^{2+}, Si^{3+}) decreased in thickness.

With respect to pure germanium, a good quality and perfectly stoichiometric GeO_2 was fabricated via atomic layer deposition (ALD) based on a divalent Ge precursor combined with O_3 [65]. Here, the O_3 was crucial to transform the chemisorbed divalent Ge precursor into tetravalent Ge on the growing surface. Ozone has also been successfully used to passivate germanium in order to engineer a Ge/insulator interface [66].

In the low temperature oxidation of silicon carbide, O_3 exhibited a much higher oxidation rate than O_2. In addition, the oxidation in ozone reduced the carbon content in the SiO_2 film, which is favourable for device operations [54].

Ozone's oxidizing abilities have also been studied with respect to different structures of carbon, most notably graphene [67], carbon nanotubes [68, 69], and, due to the effect of surface transfer doping, increasingly important diamond surfaces [70–74].

5.2. High-κ materials

Metal oxides are heavily investigated as replacements for SiO_2 in complementary metal-oxide-semiconductor (CMOS) devices, since these oxides (high-κ materials) have a higher dielectric constant. In general, using O_3 in the oxidation or ALD of three of the most promising metal oxides (Zr, Hf, Al) exhibited improved electrical characteristics over chemical methods or oxidation in O_2.

Ozone has been studied with respect to formation of zirconium oxide (ZrO_2) [75–78], where the ozone-grown oxide resulted in improved electrical characteristics over oxidation in O_2 [76] and a chemical oxide [77]. Similarly, a study of the physical and electrical properties of HfSiON confirmed that UV/O_3 forms a high quality oxide even at room temperature [79].

High quality hafnium oxide (HfO_2) has been grown on top of silicon using ozone [80–84]. HfO_2 films grown by ALD

with O_3 as oxidant yielded superior electrical characteristics, including a lower fixed charge density, a lower interface trap density, and lower leakage current density, compared to H_2O as oxidant [80]. Even though, it was found that during the oxidation process ozone formed an undesired interfacial silicate between HfO_2 and the silicon substrate [80, 81, 83], ozone allowed a better control of this interfacial layer than regular O_2 [81]. XPS data indicated that the introduction of O_3 significantly improved the bonding characteristics between hafnium and oxygen even at low temperature [84].

In the case of alumina [85, 86], the ozone-grown aluminium oxide layer was more dense and superior in its corrosion properties compared to the natural oxide [85]. The electrical characteristics of a HfAlON dielectric with a UV/O_3 interfacial oxide were superior over an interfacial chemical oxide [87].

Room temperature oxidation in UV/O_3 exhibited enhanced oxidation rates for growth of zirconia, hafnia, and alumina with oxidation rates as follows: Zr > Hf > Al [88]. To explain the enhancement by UV-light radiation during the oxidation of metals such as Zr a theoretical model has been devised which gives trends consistent with experiments [89]. Here, the tunnel electron current due to UV-light excitation plays a key role to enhance the oxidation process.

6. Summary

In this topical review we have summarized key issues relating to the oxidation of silicon by ozone, including the various types of ozone generator developed over the last twenty years, the unique (and advantageous) characteristics of ozone-grown silicon oxide, and known details of the growth process itself. Notably, SiO_2 grown by exposure to ozone has been shown to possess a diminished suboxide transition layer, reduced strain, and greater reliability. Furthermore, the oxide growth rate under ozone is independent of the crystal facet exposed, and oxidation can even occur readily on hydrogen-passivated surfaces. As an alternative oxidant to regular dioxygen, ozone presents a variety of benefits, going beyond the immediate case of silicon oxidation, and clearly warrants further study.

Acknowledgments

The authors would like to thank Akira Kurokawa, Hiroshi Itoh and Hidehiko Nonaka of AIST and Naoto Kameda of Meidensha Corporation for their fruitful comments and valuable discussions. Toshiyuki Fujimoto of NMIJ at AIST is also acknowledged to promote this international collaboration. To acknowledge financial support, SJJ is sponsored by a Royal Society University Research Fellowship and CKF has been supported by a studentship from The Leverhulme Trust.

References

[1] Hirose K, Nohira H, Azuma K and Hattori T 2007 Photoelectron spectroscopy studies of SiO_2/Si interfaces *Prog. Surf. Sci.* **82** 3–54

[2] Engel T 1993 The interaction of molecular and atomic oxygen with Si(100) and Si(111) *Surf. Sci. Rep.* **18** 91–144

[3] Green M L, Gusev E P, Degraeve R and Garfunkel E L 2001 Ultrathin (<4 nm) SiO_2 and Si–O–N gate dielectric layers for silicon microelectronics: understanding the processing, structure, and physical and electrical limits *J. Appl. Phys.* **90** 2057–121

[4] Ichimura S, Nonaka H, Morikawa Y, Noyori T, Nishiguchi T and Kekura M 2004 Development of a continuous generation/supply system of highly concentrated ozone gas for low-temperature oxidation process *J. Vac. Sci. Technol.* A **22** 1410–4

[5] Nishiguchi T, Saitoh S, Kameda N, Morikawa Y, Kekura M, Nonaka H and Ichimura S 2007 Rapid oxidation of silicon using UV-light irradiation in low-pressure, highly concentrated ozone gas below 300 C *Japan. J. Appl. Phys.* **46** 2835–9

[6] Oyama S T 2000 Chemical and catalytic properties of ozone *Catal. Rev. Sci. Eng.* **42** 279–322

[7] Chao S C, Pitchai R and Lee Y H 1989 Enhancement in thermal oxidation of silicon by ozone *J. Electrochem. Soc.* **136** 2751–2

[8] Kazor A and Boyd I W 1993 Ozone oxidation of silicon *Electron. Lett.* **29** 115–6

[9] Kazor A and Boyd I W 1993 Ozone-induced rapid low-temperature oxidation of silicon *Appl. Phys. Lett.* **63** 2517–9

[10] Hosokawa S and Ichimura S 1991 Ozone jet generator as an oxidizing reagent source for preparation of superconducting oxide thin film *Rev. Sci. Instrum.* **62** 1614–9

[11] Koike K, Fukuda T, Ichimura S and Kurokawa A 2000 High-concentration ozone generator for oxidation of silicon operating at atmospheric pressure *Rev. Sci. Instrum.* **71** 4182–7

[12] Nakamura K and Ichimura S 2005 Vibrational spectroscopic study of the interface of SiO_2/Si(100) fabricated by highly concentrated ozone: direct evidence for less strained Si–O–Si bond angle *Japan. J. Appl. Phys.* **44** 7602–4

[13] Awaji N, Ohkubo S, Nakanishi T, Sugita Y, Takasaki K and Komiya S 1996 High-density layer at the SiO_2/Si interface observed by difference x-ray reflectivity *Japan. J. Appl. Phys.* **35** L67–70

[14] Nakamura K, Kurokawa A and Ichimura S 1999 Hydrofluoric acid etching of ultra thin silicon oxide film fabricated by high purity ozone *Thin Solid Films* **343/344** 361–4

[15] Kurokawa A, Nakamura K, Ichimura S and Moon D W 2000 Reduction of the interfacial Si displacement of ultrathin SiO_2 on Si(100) formed by atmospheric-pressure ozone *Appl. Phys. Lett.* **76** 493–5

[16] Chang H S, Choi S M, Moon D W and Hwang H 2002 Improved reliability characteristics of ultrathin SiO_2 grown by low temperature ozone oxidation *Japan. J. Appl. Phys.* **41** 5971–3

[17] Kameda N, Nishiguchi T, Morikawa Y, Kekura M, Nonaka H and Ichimura S 2007 High quality gate dielectric film on poly-silicon grown at room temperature using UV light excited ozone *J. Electrochem. Soc.* **154** H769–72

[18] Cui Z J, Madsen J M and Takoudis C G 2000 Rapid thermal oxidation of silicon in ozone *J. Appl. Phys.* **87** 8181–6

[19] Eliasson B and Kogelschatz U 1991 Modeling and applications of silent discharge plasmas *IEEE Trans. Plasma Sci.* **19** 309–23

[20] Ichimura S, Hosokawa S, Nonaka H and Arai K 1991 Evaluation of new ozone generator designed for oxide film formation by molecular beam epitaxy method *J. Vac. Sci. Technol.* A **9** 2369–73

[21] Nishiguchi T, Morikawa Y, Kekura M, Miyamoto M, Nonaka H and Ichimura S 2002 Reactive oxygen beam generation system using pulsed laser evaporation of highly concentrated solid ozone *Rev. Sci. Instrum.* **73** 1217–23

[22] Tosaka A, Nishiguchi T, Nonaka H and Ichimura S 2005 Low-temperature oxidation of silicon using UV-light-excited ozone *Japan. J. Appl. Phys.* **44** L1144–6

[23] Kazor A and Boyd I W 1992 Low temperature photo-assisted oxidation of silicon *Appl. Surf. Sci.* **54** 460–4

[24] Ishikawa Y, Shibamoto T and Nakamichi I 1992 Low-temperature oxidation of silicon in dry O_2 ambient by UV-irradiation *Japan. J. Appl. Phys.* **31** 1148–52

[25] Tosaka A, Nonaka H, Ichimura S and Nishiguchi T 2007 Reaction analysis of initial oxidation of silicon by UV-light-excited ozone and the application to rapid and uniform SiO_2 film growth *J. Appl. Phys.* **101** 034909–7

[26] Kazor A, Gwilliam R and Boyd Ian W 1994 Growth rate enhancement using ozone during rapid thermal oxidation of silicon *Appl. Phys. Lett.* **65** 412–4

[27] Nakamura K, Ichimura S, Kurokawa A, Koike K, Inoue G and Fukuda T 1999 Ultrathin silicon oxide film on Si(100) fabricated by highly concentrated ozone at atmospheric pressure *J. Vac. Sci. Technol.* A **17** 1275–9

[28] Nakamura K, Ichimura S, Kurokawa A and Koike K 2002 Effect of highly concentrated ozone on the etching properties of preoxide films on Si(100) *Japan. J. Appl. Phys.* 2 **41** L754–7

[29] Ichimura S, Kurokawa A, Nakamura K, Itoh H, Nonaka H and Koike K 2000 Ultrathin SiO_2 film growth on Si by highly concentrated ozone *Thin Solid Films* **377/378** 518–24

[30] Chang H S, Choi S, Yang H, Min K Y, Moon D W, Lee H-I and Hwang H 2002 Effect of Si lattice strain on the reliability characteristics of ultrathin SiO_2 on a 4° tilted wafer *Appl. Phys. Lett.* **80** 386–8

[31] Queeney K T, Weldon M K, Chang J P, Chabal Y J, Gurevich A B, Sapjeta J and Opila R L 2000 Infrared spectroscopic analysis of the Si/SiO_2 interface structure of thermally oxidized silicon *J. Appl. Phys.* **87** 1322–30

[32] Giustino F and Pasquarello A 2005 Infrared spectra at surfaces and interfaces from first principles: evolution of the spectra across the Si(100)-SiO_2 interface *Phys. Rev. Lett.* **95** 187402–4

[33] Nishiguchi T, Nonaka H, Ichimura S, Morikawa Y, Kekura M and Miyamoto M 2002 High-quality SiO_2 film formation by highly concentrated ozone gas at below 600°C *Appl. Phys. Lett.* **81** 2190–2

[34] Deal B E and Grove A S 1965 General relationship for the thermal oxidation of silicon *J. Appl. Phys.* **36** 3770–8

[35] Baumvol I J R 1999 Atomic transport during growth of ultrathin dielectrics on silicon *Surf. Sci. Rep.* **36** 1–166

[36] Stoneham A M, Gavartin J L and Shluger A L 2005 The oxide gate dielectric: do we know all we should? *J. Phys.: Condens. Matter* **17** S2027–49

[37] Nishiguchi T, Morikawa Y, Miyamoto M, Nonaka H and Ichimura S 2001 Enhanced oxidation of silicon using a collimated hyperthermal ozone beam *Appl. Phys. Lett.* **79** 382–4

[38] Itoh H, Nakamura K, Kurokawa A and Ichimura S 2001 Initial oxidation process by ozone on Si(100) investigated by scanning tunneling microscopy *Surf. Sci.* **482/484** 114–20

[39] Narushima T, Kitajima M, Itakura A N, Kurokawa A, Ichimura S and Miki K 2007 Etching-enhanced surface stress relaxation during initial ozone oxidation *Surf. Sci.* **601** 1384–8

[40] Trenhaile B R, Agrawal A and Weaver J H 2006 Oxygen atoms on Si(100)-(2×1): imaging with scanning tunneling microscopy *Appl. Phys. Lett.* **89** 151917

[41] Fink C K and Jenkins S J 2008 First-principles molecular dynamics of the initial oxidation of Si001 by ozone *Phys. Rev.* B **78** 195407

[42] Ciacchi L C and Payne M C 2005 First-principles molecular-dynamics study of native oxide growth on Si(001) *Phys. Rev. Lett.* **95** 196101

[43] Hemeryck A, Richard N, Esteve A and Djafari Rouhani M 2007 Active oxidation: silicon etching and oxide decomposition basic mechanisms using density functional theory *Surf. Sci.* **601** 2082–8

[44] Kurokawa A and Ichimura S 1995 X-ray photoelectron spectroscopy (XPS) analysis of oxide formation on silicon with high-purity ozone *Japan. J. Appl. Phys.* **34** L1606–8

[45] Kurokawa A and Ichimura S 1996 High purity ozone oxidation on hydrogen passivated silicon surface *Appl. Surf. Sci.* **100/101** 436–9

[46] Kurokawa A, Narushima T, Nakamura K, Nonaka H, Ichimura S, Itakura A N and Kitajima M 2004 Relationship between ozone oxidation and stress evolution on an H-terminated Si surface *Japan. J. Appl. Phys.* **43** 281–6

[47] Fink C K and Jenkins S J 2008 Radical-mediated adsorption: ozone oxidation of passivated silicon *Surf. Sci.* **602** L100–3

[48] Fink C K 2008 Highly-reactive dissociative adsorption: molecular dynamics of ozone on silicon and diamond surfaces *PhD Thesis* University of Cambridge

[49] Bulanin K, Alexeev A, Bystrov D, Lavalley J and Tsyganenko d A A 1994 IR study of ozone adsorption on SiO_2 *J. Phys. Chem.* **98** 5100–3

[50] Ikeda H, Hotta K, Yamada T, Zaima S, Iwano H and Yasuda Y 1995 Oxidation of H-terminated Si(100) surfaces studied by high-resolution electron energy loss spectroscopy *J. Appl. Phys.* **77** 5125–9

[51] Cui Z J and Takoudis C G 2003 Initial oxidation of H-terminated Si(100) in O_3 (950 ppm)/O_2 and pure O_2 *J. Electrochem. Soc.* **150** G694–701

[52] Fujiwara H 2007 Initial oxidation of hydrogen-terminated silicon surface by ozone *MSc Thesis* Tokyo University of Science and AIST

[53] Maeda T, Kurokawa A, Sakamoto K, Ando A, Itoh H and Ichimura S 2001 Atomic force microscopy observation of layer-by-layer growth of ultrathin silicon dioxide by ozone gas at room temperature *J. Vac. Sci. Technol.* B **19** 589–92

[54] Narushima T, Kato M, Murase S, Ouchi C and Iguchi Y 2002 Oxidation of silicon and silicon carbide in ozone-containing atmospheres at 973 K *J. Am. Ceram. Soc.* **85** 2049–55

[55] Boyd I W, Craciun V and Kazor A 1993 Vacuum-ultra-violet and ozone induced oxidation of silicon and silicon–germanium *Japan. J. Appl. Phys.* **32** 6141–6

[56] Hamann D R 1998 Diffusion of atomic oxygen in SiO_2 *Phys. Rev. Lett.* **81** 3447–50

[57] Jin Y-G and Chang K J 2001 Mechanism for the enhanced diffusion of charged oxygen ions in SiO_2 *Phys. Rev. Lett.* **86** 1793–6

[58] Nakamura K, Kurokawa A and Ichimura S 2000 Initial oxidation of Si(100)2 x 1 by ozone: transition of growth kinetics from adsorption to ultrathin film growth *Japan. J. Appl. Phys.* **39** L357–9

[59] Koike K, Izumi K, Nakamura S, Inoue G, Kurokawa A and Ichimura S 2005 Synthesis of silicon dioxide film using high-concentration ozone and evaluation of the film quality *J. Electron. Mater.* **34** 240–7

[60] Nishiguchi T, Morikawa Y, Kekura M, Miyamoto M, Nonaka H and Ichimura S 2002 Enhanced silicon oxidation by a hyperthermal beam obtained from laser evaporation of solid ozone *J. Electrochem. Soc.* **149** F29–34

[61] Kaspar T, Tuan A, Tonkyn R, Hess W P, Rogers J W Jr and Ono Y 2003 Role of $O(^1D)$ in the oxidation of Si(100) *J. Vac. Sci. Technol.* B **21** 895–9

[62] Narushima T, Itakura A N, Kurashina T, Kawabe T and Kitajima M 2000 *Appl. Surf. Sci.* **159/160** 25–9

[63] Nakamura K, Kurokawa A and Ichimura S 1997 Comparison of initial oxidation of Si(111)77 with ozone and oxygen investigated by second harmonic generation *J. Vac. Sci. Technol.* A **15** 2441–5

[64] Madsen J M, Cui Z J and Takoudis C G 2000 Low temperature oxidation of SiGe in ozone: ultrathin oxides *J. Appl. Phys.* **87** 2046–51

[65] Perego M, Scarel G, Fanciulli M, Fedushkin I L and Skatova A A 2007 Fabrication of GeO_2 layers using a divalent Ge precursor *Appl. Phys. Lett.* **90** 162115–3
[66] Kuzum D, Krishnamohan T, Pethe A J, Okyay A K, Oshima Y, Sun Y, McVittie J P, Pianetta P A, McIntyre P C and Saraswat K C 2008 Ge-interface engineering with ozone oxidation for low interface-state density *IEEE Electron Device Lett.* **29** 328–30
[67] Maranzana A, Serra G, Giordana A, Tonachini G, Barco G and Causa M 2005 Ozone interaction with polycyclic aromatic hydrocarbons and soot in atmospheric processes: theoretical density functional study by molecular and periodic methodologies *J. Phys. Chem.* A **109** 10929–39
[68] Picozzi S, Santucci S, Lozzi L, Valentini L and Delley B 2004 Ozone adsorption on carbon nanotubes: the role of Stone–Wales defects *J. Chem. Phys.* **120** 7147–52
[69] Simmons J M, Nichols B M, Baker S E, Marcus M S, Castellini O M, Lee C-S, Hamers R J and Eriksson M A 2006 Effect of ozone oxidation on single-walled carbon nanotubes *J. Phys. Chem.* B **110** 7113–8
[70] Alvarez J, Kleider J P, Snidero E, Bergonzo P, Tromson D and Mer C 2004 On the metastability of the surface conductivity in hydrogen-terminated polycrystalline CVD diamond *Diamond Relat. Mater.* **13** 751–4
[71] Riedel M, Ristein J and Ley L 2004 The impact of ozone on the surface conductivity of single crystal diamond *Diamond Relat. Mater.* **13** 746–50
[72] Petrini D and Larsson K 2008 Theoretical study of the thermodynamic and kinetic aspects of terminated (111) diamond surfaces *J. Phys. Chem.* C **112** 3018–26
[73] Sakai T, Song K-S, Kanazawa H, Nakamura Y, Umezawa H, Tachiki M and Kawarada H 2003 Ozone-treated channel diamond field-effect transistors *Diamond Relat. Mater.* **12** 1971–5
[74] Fink C K and Jenkins S J 2009 submitted
[75] Ramanathan S, Wilk G D, Muller D A, Park C-M and McIntyre P C 2001 Growth and characterization of ultrathin zirconia dielectrics grown by ultraviolet ozone oxidation *Appl. Phys. Lett.* **79** 2621–3
[76] Ramanathan S, Muller D A, Wilk G D, Park C M and McIntyre P C 2001 Effect of oxygen stoichiometry on the electrical properties of zirconia gate dielectrics *Appl. Phys. Lett.* **79** 3311–3
[77] Ramanathan S, Park C-M and McIntyre P C 2002 Electrical properties of thin film zirconia grown by ultraviolet ozone oxidation *J. Appl. Phys.* **91** 4521–7
[78] Ramanathan S and McIntyre P C 2002 Ultrathin zirconia/SiO_2 dielectric stacks grown by ultraviolet–ozone oxidation *Appl. Phys. Lett.* **80** 3793–5
[79] Pant G, Punchaipetch P, Kim M J, Wallace R M and Gnade B E 2004 Low temperature UV/ozone oxidation formation of HfSiON gate dielectric *Thin Solid Films* **460** 242–6
[80] Park H B *et al* 2003 Comparison of HfO_2 films grown by atomic layer deposition using $HfCl_4$ and H_2O or O_3 as the oxidant *J. Appl. Phys.* **94** 3641–7
[81] Wang L, Xue K, Xu J B, Huang A P and Chu P K 2006 Control of interfacial silicate between HfO_2 and Si by high concentration ozone *Appl. Phys. Lett.* **88** 072903
[82] Chen S-C, Chen Y-Y, Chang Y-T, Lou J-C, Kin K-T and Chien C-H 2007 Improvements of ozone surface treatment on the electrical characteristics and reliability in HfO_2 gate stacks *Microelectron. Eng.* **84** 1898–901
[83] Wang Y, Dai M, Ho M-T, Wielunski L S and Chabal Y J 2007 Infrared characterization of hafnium oxide grown by atomic layer deposition using ozone as the oxygen precursor *Appl. Phys. Lett.* **90** 022906
[84] Wang L, Chu P K, Anders A and Cheung N W 2008 Effects of ozone oxidation on interfacial and dielectric properties of thin HfO_2 films *J. Appl. Phys.* **104** 054117
[85] Kuznetsova A, Yates J T Jr, Zhou G, Yang J C and Chen X 2001 Making a superior oxide corrosion passivation layer on aluminum using ozone *Langmuir* **17** 2146–52
[86] Elliott S D, Scarel G, Wiemer C, Fanciulli M and Pavia G 2006 Ozone-based atomic layer deposition of alumina from TMA: Growth, morphology, and reaction mechanism *Chem. Mater.* **18** 3764–73
[87] Chen Y-Y, Fu W-Y and Yeh C-F 2008 Electrical characteristics of the HfAlON gate dielectric with interfacial UV-ozone oxide *IEEE Electron Device Lett.* **29** 60–2
[88] Ramanathan S, Chi D, McIntyre P C, Wetteland C J and Tesmer J R 2003 Ultraviolet-ozone oxidation of metal films *J. Electrochem. Soc.* **150** F110–5
[89] Chang C-L and Ramanathan S 2007 A theoretical approach to investigate low-temperature nanoscale oxidation of metals under UV radiation *J. Electrochem. Soc.* **154** G160–4